Efa6 protects axons and regulates their growth and branching through eliminating off-track microtubules at the cortex

Yue Qu*[,1], Ines Hahn*[,#,1], Meredith Lees[1], Jill Parkin[1], André Voelzmann[1], Karel Dorey[1], Alex Rathbone[2], Claire Friel[2], Viki Allan[1], Pilar Okenve-Ramos[3], Natalia Sanchez-Soriano[3], Andreas Prokop[1,#]

1) The University of Manchester, Manchester Academic Health Science Centre, Faculty of Biology, Medicine and Health, School of Biology, Manchester, UK
2) The University of Nottingham, School of Life Sciences, Faculty of Medicine & Health Sciences, Nottingham, UK
3) Department of Cellular and Molecular Physiology, Institute of Translational Medicine, University of Liverpool, Liverpool, United Kingdom

Running title**:** The role of Efa6 in axon maintenance

Key words: *Drosophila*, neurodegeneration, axons, actin, cytoskeleton, microtubules

* authors contributed equally
# authors for correspondence:
The University of Manchester
Faculty of Life Sciences
Oxford Road
Manchester M13 9PT
Tel: +44-(0)161-27-51556
Fax: +44-(0)161-27-51505
Andreas.Prokop@manchester.ac.uk
Ines.Hahn@manchester.ac.uk

Summary statement (30 words max):

The cortical collapse factor Efa6 restricts microtubules polymerising away from axonal bundles. Thereby it limits axon growth and branching, but preserves microtubule bundle organisation crucial for axon maintenance.

Abstract

Cortical collapse factors eliminate microtubules extending towards plasma membranes, with important roles also in neurons. This is suggested by the Arf activator Efa6 in *C. elegans* important for axon growth and regeneration, and mammalian kinesin Kif21A linked to a neurodevelopmental disorder in mammals. To understand cortical collapse factor functions at the subcellular level, we studied *Drosophila* Efa6, capitalising on the experimentally and genetically amenable neurons of fruit flies. First, we show that *Drosophila* Efa6 is membrane-associated and can eliminate MTs, primarily mediated by an N-terminal 18 amino acid motif; if detached from the membrane, it can abolish entire microtubule networks in mouse fibroblasts and eliminate whole axons of fly neurons. We find that endogenous Efa6 in neurons acts as a cortical collapse factor, eliminating mainly those MTs that

leave axonal bundles and are able to contribute to morphogenetic processes. Loss of Efa6 causes an increase in such peripheral microtubules; in growth cones, this correlates with enhanced axon growth; in axons, it correlates with excessive branching and the occurrence of pathological perturbations of axonal microtubule bundles - both in neuronal cultures and *in vivo*. Efa6 over-expression causes the opposite phenotypes. Therefore, our work conceptually links sub-cellular functions of cortical collapse factors to axon growth regulation and reveals new roles in axon branching and in the prevention of axonal atrophy.

Introduction

Axons are the cable-like neuronal extensions that wire the nervous system. They are typically 0.5-10 µm in diameter, but can be up to a meter long in humans (Debanne et al., 2011; Prokop, 2013a). It is a fascinating challenge to understand how axons can extend over these enormous distances and branch in orderly manners, but also how these delicate structures can be maintained for a lifetime, i.e. many decades in humans. It is not surprising that we gradually lose about half of our axons towards old age (Calkins, 2013; Marner et al., 2003) and that axon decay is a prominent neurodegenerative phenomenon (Adalbert and Coleman, 2012; Fang and Bonini, 2012; Medana and Esiri, 2003; Wang et al., 2012).

Continuous parallel bundles of microtubules (MTs) run along the entire length of axons; these bundles provide (1) structural support, (2) highways for life-sustaining cargo transport between the cell bodies and synaptic endings, and (3) a source of MTs that can leave these bundles to drive morphogenetic changes. Through being organised in this way, MTs essentially regulate axon growth, branching and maintenance (Hahn et al., 2019; Prokop, 2013a; Prokop et al., 2013).

Axon growth during early stages of neuronal development occurs in amoeboid structures at the tips of axons called growth cones (GCs). In GCs, single MTs emanate from the axonal bundle tips (located in the GC centre) to splay into the periphery of GCs and their filopodia; peripheral stabilisation of these explorative MTs can trigger elongation of the entire MT bundle into this direction (Dent et al., 2011; Lowery and van Vactor, 2009; Prokop et al., 2013).

Axon branching can occur through parallel growth events in one growth cone, thus leading to a split and bifurcation into branches (Acebes and Ferrus, 2000). Alternatively, branching can also occur along axon shafts through MTs that leave the parallel axonal bundles and polymerise off-track towards the periphery, where they can get stabilised to seed new collateral branches (Kalil and Dent, 2014; Lewis et al., 2013; Tymanskyj et al., 2017; Yu et al., 2008).

Axon maintenance requires that MTs retain their parallel organisation into bundles; MTs that polymerise away from the bundle might pose a risk in that they can seed areas of MT disorganisation, as proposed by the model of "local axon homeostasis" (Hahn et al., 2019; Prokop, 2016; Voelzmann et al., 2016a). This model proposes that the force-enriched environment of axons promotes "off track" MTs, and active regulation through MT-binding proteins is required to "tame" them into bundled conformation. For example, the spectraplakin Short stop (Shot) promotes MT bundles through cross-linking cortical actin to the tips of polymerising MTs, thus guiding MT extension parallel to the axon (Alves-Silva et al., 2012). Consequently, the loss of spectraplakins in fly (Shot) or mouse (ACF7, dystonin/BPAG1) causes severe axonal swellings and MT disorganisations, which is a likely cause for human dystonin-linked HSAN6 ('type 6 hereditary sensory and autonomic neuropathy'; Bernier and Kothary, 1998; Dalpe et al., 1998; Sánchez-Soriano et al., 2009). Pathological axon swellings with disorganised MTs can also be observed in ageing (Fiala et al., 2007), spastin-linked 'type 4 spastic paraplegia' (Fassier et al., 2013; Tarrade et al., 2006) and Alzheimer's disease models (Adalbert et al., 2009), further supporting the importance

of MT bundle maintenance.

It is therefore of important that MTs are regulated to either bundle up or splay out. However, our knowledge of the underpinning genetic regulation remains sparse. To explore these mechanisms, we use neurons of the fruit fly *Drosophila melanogaster* as an effective model (Prokop et al., 2013). Here we focus on the axonal roles of cortical collapse factors, which are membrane-associated proteins that can eliminate MTs approaching the cell surface. Previous reports suggested important roles for cortical collapse factors in axonal biology. For example, the ARF activator Efa6 in *C. elegans* negatively impacts on developmental and regenerative axon growth mediated by its N-terminal 18 amino acid (18aa) motif (Chen et al., 2015; Chen et al., 2011; O'Rourke et al., 2010). Also, the mammalian type 4 kinesin, KIF21A, which functions as a cortical collapse factor in non-neuronal cells, influences axonal morphogenesis: in mouse hippocampal neurons, the pathogenic *KIF21A*^{R954W} mutation (linked to neurodevelopmental eye movement disorder congenital fibrosis of extraocular muscles; OMIM reference #135700; Heidary et al., 2008; Tiab et al., 2004) causes a shift of the protein away from the axon shaft to growth cones, correlating with axonal growth inhibition (van der Vaart et al., 2013).

Here we study *Drosophila* Efa6. Using gain- and loss-of-function manipulations, we show that Efa6 eliminates MTs that polymerise towards the leading edge of GCs, or away from the MT bundle towards the cortex in axon shafts. As a unifying theme, Efa6 loss causes a rise in off-track MTs leading to extra axonal growth, more axonal branching and the occurrence of pathological axonal swellings containing disorganised MTs both in cultured neurons and *in vivo*. Efa6 is therefore a cortical collapse factor necessary for accurate neuronal development and the prevention of axonal MT bundle disintegration. The function of Efa6 in preventing MT disorganisation occurs complementary to the guidance roles of the spectraplakin Shot, which suggests to us that cortical collapse factors can act as quality control factors precluding axon degeneration by containing accidental off-track MTs.

Methods

Fly stocks

Loss-of-function mutant stocks used in this study were the two deficiencies uncovering the *Efa6* locus *Df(3R)Exel6273* (94B2-94B11 or 3R:22,530,780..22,530,780) and *Df(3R)ED6091i* (94B5-94C4 or 3R:22,587,681..22,587,681), *shot*^{3} (the strongest available allele of *short stop*; Kolodziej et al., 1995; Sánchez-Soriano et al., 2009), and the null mutant alleles *Efa6*$^{KO\#1}$, *Efa6*$^{GX6[w-]}$, *Efa6*$^{GX6[w+]}$ and *Arf51F*$^{GX16[w-]}$ (all genomically engineered precise deletions; Huang et al., 2009). Gal4 driver lines used were the pan-neuronal lines *sca-Gal4* (strongest in embryos; Sánchez-Soriano et al., 2010) and *elav-Gal4* (1st and 3rd chromosomal, both expressing at all stages; Luo et al., 1994), as well as the *ato-Gal4* line expressing in a subset of neurons in the adult brain (Hassan et al., 2000; Voelzmann et al., 2016b). Lines for targeted gene expression were *UAS-Efa6*^{RNAi} (VDRC #42321), *UAS-Gal80*^{ts} (Zeidler et al., 2004), *UAS-Eb1-GFP* (Alves-Silva et al., 2012), *UAS-*α*-tubulin84B* (Grieder et al., 2000) and *UAS-tdTomato* (Zschätzsch et al., 2014). Efa6 expression was detected via the genomically engineered *Efa6-GFP* allele, where a GFP was inserted after the last amino acid in exon 14 (Huang et al., 2009).

Drosophila primary cell culture

Drosophila primary neuron cultures were performed as published previously (Prokop et al., 2012; Qu et al., 2017). In brief, stage 11 embryos were treated for 1 min with bleach to remove the chorion, sterilized for ~30 s in 70% ethanol, washed in sterile Schneider's/FCS, and eventually homogenized with micro-pestles in 1.5 centrifuge tubes containing 21 embryos per 100 µl dispersion medium

(Prokop et al., 2012) and left to incubated for 5 min at 37°C. Cells are washed with Schneider's medium (Gibco), spun down for 4 mins at 650 g, supernatant was removed and cells re-suspended in 90 µl of Schneider's medium containing 20% fetal calf serum (Gibco). 30 µl drops were placed on cover slips. Cells were allowed to adhere for 90-120 min either directly on glass or on cover slips coated with a 5 µg/ml solution of concanavalin A, and then grown as a hanging drop culture for hours or days at 26°C as indicated.

To abolish maternal rescue of mutants, i.e. masking of the mutant phenotype caused by deposition of normal gene product from the healthy gene copy of the heterozygous mothers in the oocyte (Prokop, 2013b), we used a pre-culture strategy (Prokop et al., 2012; Sánchez-Soriano et al., 2010) where cells were kept for 5 days in a tube before they were plated on a coverslip.

For the transfection of *Drosophila* primary neurons, a quantity of 70-75 embryos per 100 µl dispersion medium was used. After the washing step and centrifugation, cells were re-suspended in 100 µl transfection medium [final media containing 0.1-0.5 µg DNA and 2 µl Lipofecatmine 2000 (L2000)]. To generate this media, dilutions of 0.1-0.5 µg DNA in 50 µl Schneider's medium and 2 µl L2000 in 50 µl Schneider's medium were prepared, then mixed together and incubated at room temperature for 5-30 mins, before being added to the cells in centrifuge tubes where they were kept for 24 hrs at 26°C. Cells were then treated again with dispersion medium, re-suspended in culture medium and plated out as described above.

For temporally controlled knock-down experiments we used flies carrying the driver construct *elav-Gal4*, the knock-down construct *UAS-Efa6-RNAi*, and the temperature-sensitive Gal4 inhibitor *UAS-Gal80^{ts}*, all in parallel. At the restrictive temperature of 19°C, Gal80^{ts} blocks Gal4-induced expression of *Efa6-RNAi*, and this repressive action is removed at the permissive temperature of 27°C where Gal80^{ts} is non-functional. Control neurons were from flies carrying only the *Gal4/Gal80* (control 1 in Fig. 7K) or only the *Efa6-RNAi* transgene (control 2).

<u>Fibroblast cell culture</u>

NIH/3T3 fibroblasts were grown in DMEM supplemented with 1% glutamine (Invitrogen), 1% penicillin/streptomycin (Invitrogen) and 10% FCS in culture dishes (100 mm with vents; Fisher Scientific UK Ltd) at 37°C in a humidified incubator at 5% CO_2. Cells were split every 2-3 d, washed with pre-warmed PBS, incubated with 4 ml of Trypsin-EDTA (T-E) at 37°C for 5 min, then suspended in 7 ml of fresh culture medium and eventually diluted (1/3-1/20 dilution) in a culture dish containing 10 ml culture media.

For transfection of NIH/3T3 cells, 2 ml cell solution (~10^5 cells per ml) were first transferred to 6-well plates, and grown overnight to double cell density. 2 µg of DNA and 2 µl Plus reagent (Invitrogen) were added to 1 ml serum-free media in a centrifuge tube, incubated for 5 mins at RT, then 6 µl Lipofectamine (Invitrogen) were added, and incubated at RT for 25 mins. Cells in the 6-well plate were washed with serum-free medium and 25 mins later DNA/Lipofectamine was mixed into the medium (1/1 dilution). Plates were incubated for 3 hrs at 37°C, washed with 2 ml PBS, 400 µl trypsin were added for 5 mins (37°C), then 3 ml complete medium; cells were suspended and added in 1 ml aliquots to 35 mm glass-bottom dishes (MatTek) coated with fibronectin [300 µl of 5 µg/ml fibronectin (Sigma-Aldrich) placed in the center of a MatTek dish for 1 hr at 37°C, then washed with PBS]; 1 ml of medium was added and cells grown for 6 hrs or 24 hrs at 37°C in a CO_2 incubator. For live imaging, the medium was replaced with 2 ml Ham's F-12 medium + 4% FCS.

Dissection of adult brains

To analyse the function of Efa6 in MT bundle integrity in medulla axons *in vivo*, flies were aged at 29°C. Flies were maintain in groups of up to 20 flies of the same gender (Stefana et al., 2017) and changed into new tubes every 3-4 days. Brain dissections were performed in Dulbecco's PBS (Sigma, RNBF2227) after briefly sedating them on ice. Dissected brains with their laminas and eyes attached were placed into a drop of Dulbecco's PBS on MatTek glass bottom dishes (P35G1.5-14C), covered by coverslips and immediately imaged with a 3i Marianas Spinning Disk Confocal Microscope.

To measure branching in *ato-Gal4 Drosophila* neurons, adult brains were dissected in Dulbecco's PBS and fixed with 4% PFA for 15 min. Antibody staining and washes were performed with PBS supplemented with 0.3% Triton X-100. Specimens were embedded in Vectashield (VectorLabs).

Immunohistochemistry

Primary fly neurons and fibroblasts were fixed in 4% paraformaldehyde (PFA) in 0.05 M phosphate buffer (PB; pH 7–7.2) for 30 min at room temperature (RT); for anti-Eb1 staining, ice-cold +TIP fix (90% methanol, 3% formaldehyde, 5 mM sodium carbonate, pH 9; stored at -80°C and added to the cells; Rogers et al., 2002) was added for 10 mins. Adult brains were dissected out of their head case in PBS and fixed with 4% PFA in PBS for 1 hr, followed by a 1hr wash in PBT.

Antibody staining and washes were performed with PBT. Staining reagents: anti-tubulin (clone DM1A, mouse, 1:1000, Sigma; alternatively, clone YL1/2, rat, 1:500, Millipore Bioscience Research Reagents); anti-DmEb1 (gift from H. Ohkura; rabbit, 1:2000; Elliott et al., 2005); anti-Elav (mouse, 1:1000, DHB); anti-GFP (goat, 1:500, Abcam); Cy3-conjugated anti-HRP (goat, 1:100, Jackson ImmunoResearch); F-actin was stained with Phalloidin conjugated with TRITC/Alexa647, FITC or Atto647N (1:100 or 1:500; Invitrogen and Sigma). Specimens were embedded in ProLong Gold Antifade Mountant.

Microscopy and data analysis

Standard documentation was performed with AxioCam monochrome digital cameras (Carl Zeiss Ltd.) mounted on BX50WI or BX51 Olympus compound fluorescent microscopes. For the analysis of *Drosophila* primary neurons, we used two well established parameters (Alves-Silva et al., 2012; Sánchez-Soriano et al., 2010a): axon length (from cell body to growth cone tip; measured using the segmented line tool of ImageJ) and the degree of MT disorganisation in axons which was either measured as binary score or ratio (percentage of neurons showing obvious MT disorganisation in their axons) or as "MT disorganisation index" (MDI; Qu et al., 2017): the area of disorganisation was measured using the freehand selection in ImageJ; this value was then divided by axon length (see above) multiplied by 0.5 µm (typical axon diameter, thus approximating the expected area of the axon if it were not disorganised). For Eb1::GFP comet counts, neurons were subdivided into axon shaft and growth cones (GC): the proximal GC border was set where the axon widens up (broader GCs) or where filopodia density increases significantly (narrow GCs). MT loss in fibroblasts was assessed on randomly chosen images of successfully transfected, GFP-expressing fibroblasts, stained for tubulin and actin. Images were derived from at least 2 independent experimental repeats performed on different days, for each of which at least 3 independent culture wells were analysed by taking a minimum of 20 images per well. Due to major differences in plasma membrane versus cytoplasmic localisation of constructs, their expression strengths could not be standardised. Assuming a comparable expression strength distribution, we therefore analyse all transfected cells

in the images and assigned them to three categories: MTs intact, damaged or gone (Fig. 3G-G''). To avoid bias, image analyses were performed blindly, i.e. the genotype or treatment of specimens was masked. To analyse ruffle formation in fibroblasts, cells were stained with actin and classified (with or without ruffles).

To assess the degree of branching, we measured axonal projections of dorsal cluster neurons in the medulla, which is part of the optic lobe in the adult brain (Hassan et al., 2000; Voelzmann et al., 2016b). These neurons were labelled by expressing *UAS-myr-tdTomato* via the *ato-Gal4* driver either alone (control), together with *UAS-Efa6*^{RNAi} or together with *UAS-Efa6-FL-GFP*. We analysed them in young brains (2-5 d after eclosure of flies from their pupal case) or old brains (15-18 d). Z-stacks of adult fly brains (optic lobe area) were taken with a Leica DM6000 B microscope and extracted with Leica MM AF Premier software. They were imaged from anterior and the number of branches was quantified manually. Branches were defined as the protrusions from the DC neuron axons in the medulla. Branches in fly primary neurons at 5DIV were also counted manually and defined as MT protrusions from main axon.

To measure MT disorganisation in the optic lobe of adult flies, *GMR31F10-Gal4* (Bloomington #49685) was used to express *UAS-α-tubulin84B-GFP* (Grieder et al., 2000) in a subset of lamina axons which projects within well-ordered medulla columns (Prokop and Meinertzhagen, 2006). Flies were left to age for 26-27 days (about half their life expectancy) and then their brains were dissected out, mounted in Mattek dishes and imaged using a 3i spinning disk confocal system at the ITM Biomedecial imaging facility at the University of Liverpool. A section of the medulla columns comprising the 4 most proximal axonal terminals was used to quantify the number of swellings and regions with disorganised MTs.

Time lapse imaging of cultured primary neurons (in Schneider's/FCS) and fibroblasts (in Ham's F-12/FCS) was performed on a Delta Vision Core (Applied Precision) restoration microscope using a [*100x/1.40 UPlan SAPO (Oil)*] objective and the Sedat Quad filter set (*Chroma #89000*). Images were collected using a Coolsnap HQ2 (Photometrics) camera. The temperature was set to 26°C for fly neurons and 37°C for fibroblasts. Time lapse movies were constructed from images taken every 2 s for 2 mins. To analyse MT dynamics, Eb1::GFP comets were tracked manually using the "manual tracking" plug-in of ImageJ.

For statistical analyses, Kruskal–Wallis one-way ANOVA with *post hoc* Dunn's test or Mann–Whitney Rank Sum Tests (indicated as P_{MW}) were used to compare groups, and $\chi 2$ tests (indicated as P_{X2}) were used to compare percentages. All raw data of our analyses are provided as supplementary Excel/Prism files.

<u>Molecular biology</u>

EGFP tags are based on pcDNA3-EGFP or pUAST-EGFP. All *Drosophila melanogaster* efa6 constructs are based on cDNA cloneIP15395 (Uniprot isoform C, intron removed). *Caenorhabditis elegans* efa-6 (Y55D9A.1a) constructs are derived from pCZGY1125-efa-6-pcr8 (kindly provided by Andrew Chisholm). *Homo sapiens* PSD1 (ENST00000406432.5, isoform 202) constructs were PCR-amplified from pLC32-hu-psd1-pcr8 vector (kindly provided by Andrew Chisholm). *Homo sapiens* PSD2 (ENST00000274710.3, isoform 201, 771aa) constructs were PCR-amplified from pLC33-hu-psd2-pcr8 vector (kindly provided by Andrew Chisholm). *Homo sapiens* PSD3 was PCR-amplified from pLC34 hu-psd3-pcr8 vector (kindly provided Andrew Chisholm). Note that the PSD3 cDNA clone is most closely related to isoform 201 (ENST00000286485.12: 513aa) and therefore lacks the putative N-terminus found in isoform 202 (ENST00000327040.12). However, the putative MTED core sequence is encoded in the C-terminal PH domain (Fig.2C), not the potential N-terminus. *Homo*

sapiens PSD4 (ENST00000441564.7, isoform 205) was PCR-amplified from pLC35-hu-psd4-pcr8 vector (kindly provided by Andrew Chisholm).The CAAX motif is derived from human KRAS. The *Dm*Efa6-NtermΔSxiP::EGFP (aa1-410) insert was synthesised by GeneArt Express (ThermoFisher). All construct were cloned using standard (SOE) PCR/ligation based methods, and constructs and inserts are detailed in Table T1. To generate transgenic fly lines, *P[acman]M-6-attB-UAS-1-3-4* constructs were integrated into *PBac{yellow[+]-attP-3B}VK00031* (Bloomington line #9748) via PhiC31 mediated recombination (outsourced to Bestgene Inc.).

final vector	**Source**	**insert**
pcDNA3-EGFP	Addgene	*XhoI*-EGFP-*XbaI*
pUAST-AscI-PacI-EGFP	this study	*KpnI, AscI, PacI*-EGFP-*XbaI*
***pUAST-DmEfa6FL-EGFP* (aa1-1387)**	this study	*KpnI, AscI*-***kozak***-Efa6 (aa1-1387)-**GSGSGS-EGFP**-*PacI, XbaI*
***P[acman]M-6-attB-UAS-1-3-4-DmEfa6FL-EGFP* (aa1-1387)**	this study	*AscI*-***kozak***-*Dm*Efa6 (aa1-1387)-**GSGSGS-EGFP**-*PacI*
***pcDNA3.1-DmEfa6FL-EGFP* (aa1-1387)**	this study	*KpnI, AscI*-***kozak***-*Dm*Efa6 (aa1-1387)-**GSGSGS-EGFP**-*PacI, XbaI*
***pUAST-DmEfa6ΔCterm-EGFP* (aa1-894)**	this study	*KpnI, AscI*-***kozak***-*Dm*Efa6Δ**Cterm** (aa1-894)-**GSGSGS-EGFP**-*PacI, XbaI*
***P[acman]M-6-attB-UAS-1-3-4-DmEfa6ΔCterm-EGFP* (aa1-894)**	this study	*AscI*-***kozak***-*Dm*Efa6Δ**Cterm** (aa1-894)-**GSGSGS-EGFP**-*PacI*
***pcDNA3.1-DmEfa6ΔCterm-EGFP* (aa1-894)**	this study	*KpnI, AscI*-***kozak***-*Dm*Efa6Δ**Cterm** (aa1-894)-**GSGSGS-EGFP**-*PacI, XbaI*
***pUAST-DmEfa6-Nterm-EGFP* (aa1-410)**	this study	*KpnI, AscI*-***kozak***-*Dm*Efa6-Nterm (aa1-410)-**GSGSGS-EGFP**-*PacI, XbaI*
***P[acman]M-6-attB-UAS-1-3-4-DmEfa6-Nterm-EGFP* (aa1-410)**	this study	*AscI*-***kozak***-*Dm*Efa6-Nterm (aa1-410)-**GSGSGS-EGFP**-*PacI*
***pcDNA3.1-DmEfa6-Nterm-EGFP* (aa1-410)**	this study	*KpnI, AscI*-***kozak***-*Dm*Efa6-Nterm (aa1-410)-**GSGSGS-EGFP**-*PacI, XbaI*
***pUAST-DmEfa6-Nterm-CAAX-EGFP* (aa1-410)**	this study	*KpnI, AscI*-***kozak***-*Dm*Efa6-Nterm (aa1-410)-**GSGSGS-EGFP-CAAX[KRAS]**-*PacI, XbaI*
***P[acman]M-6-attB-UAS-1-3-4-DmEfa6-Nterm-CAAX-EGFP* (aa1-410)**	this study	*AscI*-***kozak***-*Dm*Efa6-Nterm (aa1-410)-**GSGSGS-EGFP-CAAX[KRAS]**-*PacI*
***pcDNA3.1-DmEfa6-Nterm-CAAX-EGFP* (aa1-410)**	this study	*KpnI, AscI*-***kozak***-*Dm*Efa6-Nterm (aa1-410)-**GSGSGS-EGFP-CAAX[KRAS]**-*PacI, XbaI*
***pUAST-DmEfa6-NtermΔSxiP-EGFP* (aa1-410)**	this study	*KpnI, AscI*-***kozak***-*Dm*Efa6-NtermΔ**SxiP** (aa1-410; **SQIP>AAAA; SRIP>AAAA**)-**GSGSGS-EGFP**-*PacI, XbaI*
***pcDNA3.1-DmEfa6-NtermΔSxiP-EGFP* (aa1-410)**	this study	*KpnI, AscI*-***kozak***-*Dm*Efa6-NtermΔ**SxiP** (aa1-410; **SQIP>AAAA; SRIP>AAAA**)-**GSGSGS-EGFP**-*PacI, XbaI*
***pUAST-DmEfa6-NtermΔMTED-EGFP* (aa1-300)**	this study	*KpnI, AscI*-***kozak***-*Dm*Efa6-NtermΔ**MTED** (aa1-300)-**GSGSGS-EGFP**-*PacI, XbaI*
***pcDNA3.1-DmEfa6-NtermΔMTED-EGFP* (aa1-300)**	this study	*KpnI, AscI*-***kozak***-*Dm*Efa6-NtermΔ**MTED** (aa1-300)-**GSGSGS-EGFP**-*PacI, XbaI*
***pUAST-DmEfa6ΔNerm-EGFP* (aa851-1387)**	this study	*KpnI, AscI*-***kozak***-*Dm*Efa6Δ**Nerm** (aa851-1387)-**GSGSGS-EGFP**-*PacI, XbaI*
***pcDNA3.1-DmEfa6ΔNerm-EGFP* (aa851-1387)**	this study	*KpnI, AscI*-***kozak***-*Dm*Efa6Δ**Nerm** (aa851-1387)-**GSGSGS-EGFP**-*PacI, XbaI*
***pUAST-DmEfa6-MTED-EGFP* (aa322-341)**	this study	*KpnI, AscI*-***kozak***-*Dm*Efa6-MTED (aa322-341)-**GSGSGS-EGFP**-*PacI, XbaI*
***pcDNA3.1-DmEfa6-MTED-EGFP* (aa322-341)**	this study	*KpnI, AscI*-***kozak***-*Dm*Efa6-MTED (aa322-341)-**GSGSGS-EGFP**-*PacI, XbaI*
***pcDNA3.1-CeEfa6-FL-EGFP* (aa1-816)**	this study	*KpnI, AscI*-***kozak***-*Ce*Efa6 (aa1-816)-**GSGSGS-EGFP**-*PacI, XbaI*

***pcDNA3.1-CeEfa6-Nterm-EGFP* (aa1-152)**	this study	*KpnI, AscI*-***kozak***-*Ce*Efa6-Nterm (aa1-152)-**GSGSGS-EGFP**-*PacI, XbaI*
***pcDNA3.1-CeEfa6-MTED-EGFP* (aa24-42)**	this study	*KpnI, AscI*-***kozak***-*Ce*Efa6-MTED (aa24-42)-**GSGSGS-EGFP**-*PacI, XbaI*
***pcDNA3.1-HsPSD1-FL-EGFP* (aa1-1024)**	this study	*KpnI, AscI*-***kozak***-*Hs*PSD1 (aa1-1024)-**GSGSGS**-*NotI*-**EGFP**-*PacI, XbaI*
***pcDNA3.1-HsPSD1-Nterm-EGFP* (aa1-280)**	this study	*KpnI, AscI*-***kozak***-*Hs*PSD1-Nterm (aa1-280)-**GSGSGS**-*NotI*-**EGFP**-*PacI, XbaI*
***pcDNA3.1-HsPSD1-MTED-EGFP* (aa31-49)**	this study	*KpnI, AscI*-***kozak***-*Hs*PSD1-MTED (aa31-49)-**GSGSGS**-*NotI*-**EGFP**-*PacI, XbaI*
***pcDNA3.1-HsPSD2-FL-EGFP* (aa1-771)**	this study	*KpnI, AscI*-***kozak***-*Hs*PSD2 (aa1-771)-**GSGSGS**-*NotI*-**EGFP**-*PacI, XbaI*
***pcDNA3.1-HsPSD3-EGFP* (aa515-1047)**	this study	*KpnI, AscI*-***kozak***-*Hs*PSD3 (aa515-1047)-**GSGSGS**-*NotI*-**EGFP**-*PacI, XbaI*
***pcDNA3.1-HsPSD4-FL-EGFP* (aa1-1027)**	this study	*KpnI, AscI*-***kozak***-*Hs*PSD4 (aa1-1027)-**GSGSGS**-*NotI*-**EGFP**-*PacI, XbaI*
***pcDNA3.1-co-HsPSD1-MTED-EGFP* (aa31-49)**	this study	*KpnI, AscI*-***kozak***-*Hs*PSD1-MTED (aa31-49)-**GSGSGS-EGFP**-*PacI, XbaI*
***pcDNA3.1-co-CeEfa6-MTED-EGFP* (aa24-42)**	this study	*KpnI, AscI*-***kozak***-*Ce*Efa6-MTED (aa24-42)-**GSGSGS-EGFP**-*PacI, XbaI*
***pcDNA3.1-co-DmEfa6-MTED-EGFP* (aa322-341)**	this study	*KpnI, AscI*-***kozak***-*Dm*Efa6-MTED (aa322-341)-**GSGSGS-EGFP**-*PacI, XbaI*
pCS107-DmEfa6-Nterm-EGFP	this study	*NotI*-***kozak***-*Dm*Efa6-Nterm (aa1-410)-***GSGSGS-EGFP***-*StuI*
***RFP* (*Xenopus* injection)**	tba	tba
pFastBac-His6-MCAK-EGFP-StrepII	tba	His6-MCAK::EGFP-StrepII
***pFastBac-His6-DmEfa6ΔCterm-EGFP-StrepII* (aa1-894)**	this study	His6-*Dm*Efa6Δ**Cterm**::EGFP-StrepII (aa1-894)

Tab. T1. co=codon optimised; *Dm=Drosphila melanogaster*; *Ce=Caenorhabditis elegans*; *Hs=Homo sapiens*

In silico analyses

To generate the **phylogenetic tree** of Efa6/PSD full length isoforms and N-terms of different species (see Fig. S1), their amino acid sequences were aligned using Muscle or ClustalO (Goujon et al., 2010; McWilliam et al., 2013; Sievers et al., 2011). ProtTest (Abascal et al., 2005; Darriba et al., 2011) was used to determine amino acid frequencies in the protein datasets and to identify the optimal amino acid substitution model to be used for the Bayesian inference (VT+I+G+F). CUDA-Beagle-optimised MrBayes (Ronquist et al., 2012) was run using the VT+I+G+F model [prset statefreqpr=fixed(empirical); lset rates=invgamma] using 5 chains (1 heated) and 9 parallel runs until the runs converged and standard deviation of split frequencies were below 0.015 (0.06 for N-terms); PSRF+ was 1.000 and min ESS was >1300 for the TL, alpha and pinvar parameters. The *Drosophila melanogaster* Sec7-PH domain-containing protein Steppke was used as outgroup in the full length tree. Archaeopteryx (Han and Zmasek, 2009) was used to depict the MrBayes consensus tree showing branch lengths (amino acid substitutions per site) and Bayesian posterior probabilities.

To **identify a potential MTED in PSD1**, previously identified Efa6 MTED motifs (O'Rourke et al., 2010) of 18 orthologues were aligned to derive an amino acid logo. Further orthologues were identified and used to refine the logo. Invariant sites and sites with restricted amino acid substitutions were determined (most prominently MxG-stretch). Stretches containing the invariant MxG stretch were aligned among vertebrate species to identify potential candidates. Berkley's Weblogo server (Crooks et al., 2004) was used to generate amino acid sequence logos for each phylum using MTED (ExxxMxGE/D) and MTED-like (MxGE/D) amino acid stretches.

In vitro analyses

Protein Expression and Purification: *Drosophila* Efa6-ΔCterm was cloned into a modified pFastBac vector containing an N-terminal *His6* tag and C-terminal *eGFP* and *StrepII* tags. Recombinant protein was expressed in Sf9 insect cells for 72 hours using a Baculovirus system. The protein was purified via a two-step protocol. Cleared lysate was loaded onto a 1ml HisTrap column (GE Healthcare) in Ni-Affinity buffer [50 mM Tris pH 7.5, 300 mM NaCl, 10 % (v/v) glycerol, 1 mMM was shipped as lyophilized powder with a purity of 95.2%. Upon arrival peptide was dissolved in ultrapure water and stored at -20°C.

MT binding assays: GMPCPP-stabilised, rhodamine-labeled MTs were adhered to the surface of flow chambers as described earlier (Helenius et al., 2006). 20 nM Efa6-ΔCterm::GFP (in BRB20 pH 6.9, 75mM KCl, 0.05% Tween20, 0.1 mg/ml BSA, 1% 2-mercaptoethanol, 40mM glucose, 40 mg/ml glucose oxidase, 16 mg/ml catalase), 20 nM MCAK::GFP (in the same buffer plus 1 mM ATP and 1 mM taxol) was introduced to the MT-containing channel. Images were recorded using a Zeiss Observer.Z1 microscope equipped with a Zeiss Laser TIRF 3 module, QuantEM 512SC EMCDD camera (Photometrics) and 100x objective (Zeiss, alphaPlanApo/1.46NA oil). Images of rhodamine-labeled MTs using a lamp as the excitation source and GFP fluorescence using TIRF illumination via a 488 nm laser were collected as described earlier (Patel et al., 2016). For both rhodamine and GFP imaging an exposure time of 100 ms was used. The mean GFP intensity on individual MTs was determined from the mean pixel intensity of lines drawn along the long-axis of individual microtubules in Fiji (Schindelin et al., 2012). The rhodamine signal was used to locate the position of MTs in the GFP images. Intensity from a region of background was subtracted.

MT depolymerisation assays: Single-cycled, rhodamine-labeled, GMPCPP-stabilised MTs were adhered to the surface of flow chambers as described in (Helenius et al., 2006). Images of a field of fluorescent microtubules (25% rhodamine-labeled tubulin) were recorded using a Zeiss Observer.Z1 microscope, collecting 1 image every 5 s with an exposure time of 100 ms. Efa6-ΔCterm::GFP (14 nM), MCAK (40 nM) in solution (BRB20 pH 6.9, 75mM KCl, 1mM ATP, 0.05% Tween 20, 0.1 mg/ml BSA, 1% 2-mercaptoethanol, 40mM glucose, 40 mg/ml glucose oxidase, 16 mg/ml catalase) were added to the channel 1 min after acquisition had commenced. De-polymerisation rates were determined from plots of the length of individual microtubules versus time, obtained by thresholding and particle analysis of images using Fiji (Schindelin et al., 2012).

***Xenopus* oocyte assays**: cytosol extracts from *Xenopus* oocytes were obtained as described in (Allan and Vale, 1991). **MT depolymerisation** was assessed in a microscopic flow chamber (Vale and Toyoshima, 1988) where *Xenopus* cytosol (1 µl cytosol diluted with 20 µl acetate buffer) was incubated for 20 min to allow MTs to polymerise. Then cytosol was exchanged by flow through with Efa6-ΔCterm::GFP, MCAK or synthetic MTED peptide (all 20 nM in acetate buffer pH 7.4: 100 mM K-Acetate, 3 mM Mg-Acetate, 5 mM EGTA, 10 mM HEPES), and MT length changes observed by recording 10 random fields via VE-DIC microscopy (Allan, 1993; Allan and Vale, 1991). **MT polymerisation** was analysed in a microscope flow cell containing 9 µl diluted *Xenopus* cytosol (see above) to which 1 µl acetate buffer was added, either alone or containing 20nM MTED. After 10 min, 20 random fields were recorded via VE-DIC microscopy for each condition and the numbers of MTs per field counted.

For the *in vivo* assay, *Xenopus* embryos were injected in one blastomere at the 4-cell stage with 200 ng of mRNA encoding Efa6-Nterm::GFP or mCherry alone. The embryos were imaged at stage 10.25 (Heasman, 2006) with a Leica fluorescent stereoscope.

Results

Efa6 is widely expressed in *Drosophila* neurons where it restricts axonal growth

To evaluate the function of Efa6 in neurons, we first determined its expression in the nervous system. We used a genomically engineered fly line in which the endogenous *Efa6* gene was GFP-tagged (*Efa6-GFP*; Huang et al., 2009). These animals widely express *Efa6-GFP* throughout the CNS at larval and adult stages (Fig. 1F-I). We cultured primary neurons from this fly line to analyse the subcellular distribution of Efa6. In young neurons (6 hrs *in vitro;* 6 HIV) as well as mature neurons (5 days *in vitro*; 5DIV), Efa6 was localised throughout cell bodies and axons (Fig. 1A-E).

We next determine whether *Drosophila* Efa6 has an impact on axon growth, using fly lines with decreased or abolished Efa6 expression: Efa6 knock-down (*Efa6-RNAi*), overlapping deficiencies uncovering the entire *Efa6* gene locus ($Efa6^{Def}$), or different loss-of-function mutant alleles generated by genomic engineering ($Efa6^{KO\#1}$, $Efa6^{GX6[w-]}$, $Efa6^{GX6[w+]}$). In all these conditions, axon length at 6 HIV was increased compared to wild-type by at least 20% (Fig. 2). We also generated transgenic fly lines for the targeted over-expression of GFP-tagged full length Efa6 (Efa6-FL::GFP). Upon over-expression using the pan-neuronal driver line *elav-Gal4*, Efa6-FL::GFP localised to cell bodies, axons and growth cones of primary neurons, as similarly observed with the endogenous protein (Figs.1B,C). Its expression caused a 20% reduction in axon length (2C,D). Together these results suggest that Efa6 restricts axonal growth, comparable to reports for *C. elegans* Efa6 (*Ce*Efa6; Chen et al., 2015; Chen et al., 2011).

Efa6 eliminates whole axons in fly neurons and entire MT networks in mouse fibroblasts

To assess whether the negative impact of Efa6 on axon outgrowth is due to potential MT elimination activities and to determine the potential functional domains required, we extended the use of our *Drosophila* primary neuron model by developing methods for the transfection of expression constructs (see Methods). When transfecting the *Efa6-FL-GFP* expression construct, Efa6-FL::GFP localised throughout cell bodies and axons, as similarly observed with transgenic expression of the identical protein (Figs.1C, S3B). Axon length upon transfection was even further decreased than observed with the transgenic version, likely due to higher copy numbers of the expression construct (Fig. 2D). We also noticed that Efa6-FL::GFP expression almost doubled the numbers of axon-less neurons (~43%) as compared to GFP controls (~26%; Fig.3B).

To assess potential MT inhibition properties of Efa6, we used NIH3T3 mouse fibroblasts as a heterologous cell system known to work well for neuronal *Drosophila* proteins (Alves-Silva et al., 2012; Beaven et al., 2015). When fibroblasts were analysed 24 hrs after transfection, we found a graded responses of MT networks depending on the amounts of Efa6-FL::GFP expressed (shown and quantified in Fig.S5). At moderate expression levels, Efa6-FL::GFP localised along the circumference and in areas of membrane folds (open arrow heads in Figs.S5B), and MTs tended to be lost predominantly from the cell fringes (curved arrows in Figs. S5B and S7B). At high expression levels, Efa6-FL::GFP became detectable in the cytoplasm and even nucleus (double-chevrons in Fig.S5C), suggesting that membrane-association might become saturated; in these cases, MTs were completely absent (Fig.S5C). When quantifying these MT phenotypes across all transfected fibroblasts, there was a strong increase in MT networks defects and depletion upon Efa6-FL::GFP expression as compared to GFP controls (Fig. 3B).

Taken together, our data are consistent with MT-eliminating functions of fly Efa6. The fibroblast experiments suggest that Efa6 is membrane-associated and eliminates MTs from this position, whilst

the studies in neurons indicate the relevance of such functions for neuronal morphogenesis. The combined use of mouse fibroblasts and *Drosophila* primary neurons provides therefore a robust system with informative readouts for MT loss - ideal to carry out a systematic structure-function analysis of Efa6.

The N-terminal 18aa motif of Efa6 is essential for microtubule-eliminating activity of Efa6

A detailed analysis of the domain structures and phylogenetic relationships of Efa6 proteins from 30 species revealed that all chordate proteins are rather distant from invertebrates, and that arthropods form a clear subgroup within the invertebrates (Fig. S1A). Most C-termini contain a putative pleckstrin homology domain (PH; Macia et al., 2008) likely explaining the observed membrane association in fibroblasts, a Sec7 domain (potentially activating Arf GTPases; D'Souza-Schorey and Chavrier, 2006; Huang et al., 2009) and a coiled-coil (CC) domain (Franco et al., 1999; Fig.3A, S2). In contrast, the N-termini are mainly unstructured and reveal enormous length differences among species; phylogenetic relationship analyses with the N-terminus alone result in a very similar tree as the full length comparison (Fig. S1A,B), and none of the identifiable domains/motifs is particularly well conserved (details in Fig.S2). For example, the *Drosophila* N-terminus contains (1) a putative PDZ domain (aa16-88; mainly found in insect versions of Efa6), (2) two SxIP motifs (aa 233-6 and 262-5) surrounded by positive charges expected to bind Eb1 (Honnappa et al., 2009; found primarily in Efa6 of flies, some other insects and molluscs; some vertebrate/mammalian species display derived SxLP motifs), and (3) a motif of 18aa displaying 89% similarity with a motif in the N-terminus of *Ce*Efa6 suggested to be involved in MT elimination (O'Rourke et al., 2010; conserved in nematodes, arthropods and molluscs).

To assess potential roles of the *Drosophila* 18aa motif (from now on referred to as MT elimination domain, MTED), we generated a series of GFP-tagged N-terminal constructs (Fig.3B): *Efa6-ΔCterm-GFP* (encoding the entire N-terminal half upstream of the Sec7 domain), *Efa6-Nterm-GFP* (restricting to the N-terminal part containing all the identified functional domains), *Efa6-Nterm$^{\Delta MTED}$-GFP* (lacking the MTED) and *Efa6-MTED-GFP* (encoding only the MTED). All these N-terminal Efa6 variants showed the same localisation pattern throughout neurons (Fig.S3C,D,F,G), and in the cytoplasm and nucleus of fibroblasts (Fig.S3C,D,F,G). Cytoplasmic and nuclear localisations occurred even at low expression levels, indicating that the absent C-terminus (and PH domain within) usually mediates membrane association. The nuclear localisation was unexpected in the absence of any potential nuclear localisation sequences in the N-terminus (Figs.3A, S2A), and is likely due to a known artefact of GFP-tagged proteins (Alves-Silva et al., 2012; Seibel et al., 2007).

In spite of their very similar localisation patterns, only constructs containing the MTED (Efa6-ΔCterm::GFP, Efa6-Nterm::GFP and Efa6-MTED::GFP) caused increases in neuronal axon loss and MT network depletion in fibroblasts, whereas Efa6-Nterm$^{\Delta MTED}$::GFP behaved like GFP controls (Figs.3B; S3C,D,F,G; S7C,D,G,H). This result clearly indicates that the *Drosophila* MTED is the key mediator of MT-depleting functions of Efa6. However, we noted that Efa6-MTED::GFP caused milder phenotypes than the longer Efa6-ΔCterm::GFP and Efa6-Nterm::GFP variants. This might suggest that other motifs/domains in the N-terminus might contribute.

Potential candidates for such additional domains are the two SxIP sites (Fig.3A), especially since occasional MT tip tracking was observed with Efa6-Nterm::GFP in fibroblasts, suggesting them to be functional (Suppl. Movie M1). However, when replacing each of the two SxIP motifs by four alanines (Efa6-Nterm$^{\Delta SxIP}$::GFP), we observed no obvious impact on the loss of neuronal axons or MT networks in fibroblasts (Figs.3B, S3E, S4E). This suggests that the SxIP motifs play no obvious role in enhancing MTED functions, comparable to the situation of Kif2C which is a MT tip-tracker but

does not require this property for its MT depolymerising activity (Moore et al., 2005).

To assess whether the MTED motif is a good predictor for MT-eliminating capabilities of Efa6 family members, we used a whole range of different constructs: full length versions of *Ce*Efa6, *Drosophila* Efa6 and all four human PSDs (Fig. 3C), as well as N-terminal versions of *Ce*Efa6, fly Efa6 and human PSD1 (Fig. 3D). Furthermore, we deduced a MTED consensus sequence from 39 *Efa6* genes (details in Fig. S2C), identified the most likely human MTED-like sequence [position 31-49aa of PSD1; Fig. 3A] and synthesised codon-optimised versions of this human as well as the fly and worm MTEDs (Figs. S2B,C). When transfected into fibroblasts, we found that all three fly and all three worm constructs had strong MT-eliminating properties, whereas none of the 6 human constructs (PSD1-4 full length, PSD1-Nterm, PSD1-MTED-like) showed MT collapse (Fig.3C-E). Therefore, the presence of a well conserved canonical MTED seems to be a good predictor for MT eliminating capabilities of Efa6 proteins.

Taken together, *we* provide experimental proof that the N-terminal MTED, which exists primarily in Efa6 homologues of invertebrate species, is a conserved motif mediating MT-eliminating function (O'Rourke et al., 2010).

The C-terminal domain restrict the microtubule-eliminating activity of Efa6 to the cortex

The structure-function analyses strongly suggested that Efa6 is membrane-associated. This is further supported by a membrane ruffle phenotype we observed in fibroblasts when expressing Efa6-FL::GFP or the C-terminal derivative Efa6-ΔNterm::GFP (Figs.3B; curved open arrows in Fig.S4B,H, S6B,D). Efa6-ΔNterm::GFP had now obvious effects on MT networks (Fig. S7I), and its membrane ruffling phenotype likely reflects an evolutionarily conserved function of the Efa6 C-terminus through its Sec7, PH and/or CC domains (details in Fig.S6; Derrien et al., 2002; Franco et al., 1999; Macia et al., 2008). Accordingly, we find the same membrane ruffling when expressing PSD1-FL::GFP (curved open arrows in Fig. S6E).

However, even if the C-terminus plays no active role in the MT elimination process, it still regulates this function. This is suggested by the Efa6-ΔCterm::GFP and Efa6-Nterm::GFP variants which lack the C-terminus (and PH domain within; Fig.3B): they fail to associate with the cortex (Fig.S3C,D,F,G), do not cause ruffling (Fig.S6C) but induce MT phenotypes far stronger than Efa6-FL::GFP does (Figs.3B; S7C,D,H *vs* B). To assess whether lack of membrane tethering could explain this phenotypic difference, we generated the Efa6-Nterm-GFP::CAAX variant (Fig.3B) where Efa6-Nterm::GFP is fused to the membrane-associating CAAX domain (Hancock et al., 1991). Compared to Efa6-Nterm::GFP, the addition of CAAX changed its properties back to Efa6-FL::GFP-like behaviours (Figs.3B; S4B,I; S7B,E): in fibroblasts, the hybrid protein localises to the cortex and reduced the MT phenotype; in neurons, it reduces the axon loss phenotype. These findings confirm membrane tethering as an important regulatory feature restricting Efa6 function.

Taken together, our structure-function data clearly establish *Drosophila* Efa6 as a cortical collapse factor: its N-terminal MTED displays MT-eliminating properties which are restricted to the cortex via the Efa6 C-terminus.

Efa6 negatively regulates microtubules at the growth cone membrane and in filopodia

Having verified that *Drosophila* Efa6 acts as a cortical collapse factor, we next asked how this function relates to the observed axon growth phenotypes. For this, we focussed on growth cones (GCs) as the sites where axons extend; this extension requires splaying MTs that emanate from the axonal bundle tip at the base of GCs and explore the actin-rich periphery (Dent et al., 2011; Lowery

and van Vactor, 2009; Prokop et al., 2013).

In GCs of primary neurons at 6 HIV, loss of Efa6 caused an increase in MT polymerisation events: the total number of Eb1 comets was increased as compared to wild-type controls (Fig. 4I). Eb1::GFP comets in *Efa6* mutant neurons frequently persisted when reaching the GC periphery, where they could occasionally be observed to undergo curved extensions along the periphery (Suppl. Mov. SM2-SM5). Accordingly, the lifetime of Eb1::GFP comets was ~1.4 times longer in mutant GCs, with the dwell time of Eb1 comets at the tip of filopodia being increased from ~2 s in wild-type to ~6 s in *Efa6* mutant neurons (Fig. 4M), while comet velocity was unaffected (~0.3 µm/s); we even observed cases where comets at the tips of filopodia were moving backwards, seemingly pushed back by the retracting filopodial tip (Suppl. Mov. SM3 and SM4). In agreement with the increased lifetime, more microtubules invaded growth cone filopodia in *Efa6* mutant neurons, as was quantified by counting filopodia containing EB1comets or MTs (Fig.4D,E,J,K; note that the total number of filopodia per GC was in the range of 10-11 for both wild-type and *Efa6*; not shown). Transgenically expressed Efa6-FL::GFP caused the opposite effect, i.e. a reduction in the number of GC filopodia containing Eb1 comets or MTs (green columns in Fig. 4G-L).

Next, we investigated MT dynamics in axon shafts, which clearly differ from GCs in that the majority of MTs are organised into bundles, expected to be kept away from the membrane. Accordingly, neither loss- nor gain-of-function had an obvious effect on Eb1 comet numbers, lifetimes, velocities and directionalities (Fig. 5A-D). However, like in GCs, there was a strong increase in MTs entering filopodia along the shaft upon loss of Efa6, and a strong decrease when over-expressing Efa6-FL::GFP (Fig. 5E-G).

Taken together, our data are consistent with a model in which Efa6 eliminates MTs primarily when they leave the axon bundle and polymerise towards the cell membrane or into filopodia.

Efa6 negatively regulates axon branching

Axonal MTs have been suggested to regulate branch formation by invading filopodia and stabilising them to seed new collateral branches (see Introduction; Kalil and Dent, 2014; Lewis et al., 2013). Since numbers of filopodial MTs are increased in Efa6 mutant neurons, we wondered therefore whether this might promote axonal branch formation. For this, we assessed mature primary neurons at 5 days *in vitro* (DIV). We found that *Efa6*$^{KO\#1}$ homozygous mutant neurons showed almost double the number of collateral branches than wild-type neurons, whereas expression of Efa6-FL::GFP reduced branching by 21% (Fig.6A-C,E). This reduction is suggested to be mediated by the Efa6 N-terminus, since expression of Efa6-Nterm::GFP::CAAX caused a similar degree of branch reduction (Fig.6D,E).

To extend these studies to neurons *in vivo*, we studied dorsal cluster neurons, a subset of neurons with stereotypic axonal projections in the optic lobe of adult brains (Fig.6F-K, see Methods; Hassan et al., 2000; Voelzmann et al., 2016b). To manipulate Efa6 levels in these neurons, either *Efa6-RNAi* or *Efa6-FL-GFP* was co-expressed with the membrane marker *myr-tdTomato*. Their axon branches were assessed in brains of young and old flies (2-5 d and 15-18 d after eclosure from the pupal case, respectively; Figs.6F-K). We found that *Efa6* knock-down in dorsal cluster neurons caused a significant increase in branch numbers both in young (29%) and in old brains (38%), whereas over-expression of Efa6::GFP strongly decreased branch numbers by 33% in young and 28% in old brains, respectively (Fig.6L).

In these experiments, Efa6-FL::GFP expression had an intriguing further effect: Only 57% of young brains had any axons in the medulla region, compared to 88% in controls (Figs.6H,M, S9B). However, in the older Efa6-FL::GFP expressing fly brains, the axons were eventually present (Fig.6K,M, S9D).

We concluded that this phenotype reflected delayed outgrowth, which is also consistent with the short axon growth observed upon Efa6 over-expression in primary neurons (green bars in Fig.2D).

Taken together, our data indicate Efa6 as a negative regulator of axonal branching, mediated through its N-terminus, most likely via its function as cortical collapse factor.

Efa6 maintains axonal MT bundle integrity in cultured neurons

In previous experiments we found that MT dynamics were grossly unaffected in the axons of neurons lacking Efa6. However, we noticed that a significant amount of Efa6-depleted neurons displayed axons with swellings where MTs lost their bundled conformation and were arranged into intertwined, criss-crossing curls instead (Fig.S10; arrowheads in Fig. 7D-F). To quantify the strength of this phenotype, we measured the area of MT disorganisation relative to axon length (referred to as 'MT disorganisation index', MDI; Qu et al., 2017). MDI measurements in *Efa6* mutant neurons revealed a mild 1.3 fold increase in MT disorganisation in young neurons which gradually worsened to 2.3 fold at 5 DIV and ~4 fold at 10 DIV (Fig.7A-F,I; all normalised to controls).

The observed gradual increase in phenotype could be the result of a genuine function of *Efa6* not only during axon growth but also the subsequent maintenance. Alternatively, it could be caused by maternal gene product deposited in the mutant embryos by their heterozygous mothers (Prokop, 2013b); such maternal *Efa6* could mask mutant phenotypes at early stages so that they become apparent only after most Efa6 has degraded. To assess the latter possibility, we used a pre-culture strategy to remove potential maternal Efa6 (see Methods; Prokop et al., 2012; Sánchez-Soriano et al., 2010). When plating neurons after 5 days of pre-culture, we still found a low amount of MT disorganisation in young neurons and a subsequent gradual increase to severe phenotypes over the following days (Fig.7J).

This finding argues for a continued role of Efa6 in preventing MT disorganisation during development as well as in mature neurons. To further test this possibility, we used a temperature-based conditional knock-down technique (based on GAL80^{ts}; see Methods). Using this technique, we grew the neurons for 3 days (when they have long undergone synaptic differentiation; Küppers-Munther et al., 2004; Prokop et al., 2012), before inducing *Efa6* knock-down. Following this delayed onset, cells were kept for four further days under *Efa6* knock-down conditions and fixed at day seven. We found a significant increase in MT disorganisation in the experimental neurons as compared to control neurons without knock-down (Fig. 7K). In contrast, at 3 DIV (i.e. before onset of knock-down) there was no difference in MT disorganisation between experimental and control neurons. This clearly indicates that MT disorganisation upon Efa6 deficiency occurs even in fully differentiated neurons and is not restricted to development.

In contrast to increased MT disorganisation upon Efa6 loss of function, expression of Efa6-FL::GFP for 5 days in wild-type neurons could reduce MT disorganisation even below the baseline levels measured in control cells (cultured in parallel without the expression construct; Fig.7I). We find the same trend using Efa6-Nterm::GFP::CAAX (Fig.7I), arguing that also this role of Efa6 is due to its cortical collapse function.

Efa6 maintains axonal MT bundle integrity *in vivo*

We then assessed whether a role of Efa6 in MT bundle maintenance is relevant *in vivo*. For this, we studied a subset of lamina neurons, which project prominent axons in the medulla of the adult optic lobe (Prokop and Meinertzhagen, 2006). We labelled MTs in these axons by expressing *α-tubulin84B-GFP* either alone (*GMR-tub* controls), or together with *Efa6^{RNAi}* to knock down *Efa6*

specifically in these neurons (*GMR-tub-Efa6^{IR}*; see Methods for details).

When analysing aged flies at 26-27 days, we found that Efa6 knock-down caused a doubling in the occurrence of axonal swellings with disorganised axonal MTs: the average of total swellings per column section was increased from 0.3 in controls to 0.65 swellings upon Efa6 knock-down; about a third of these contained disorganised MTs (*GMR-tub-Efa6^{IR}*: 0.23 per column section; *GMR-tub*: 0.13; Fig.8). These data demonstrated that our findings in cultured neurons are relevant *in vivo*.

We propose that Efa6 provides a quality control mechanism that prevents MT disorganisation by eliminating only MTs that have escaped axonal bundles. This model would also be consistent with the slow onset and gradual increase of MT disorganisation we observed upon Efa6 deficiency (Fig.7I,J).

<u>Efa6 and Shot cooperate in MT bundle formation and maintenance</u>

If Efa6 provides a quality control mechanism "cleaning up" accidental off-track MTs, its absence should enhance mutant phenotypes of other factors actively driving MT bundle formation. The most prominent neuronal factors actively promoting axonal MT bundles in both mammals and fly are the spectraplakins (Bernier and Kothary, 1998; Dalpe et al., 1998; Voelzmann et al., 2017). In *Drosophila*, spectraplakins are represented by the single *short stop* (*shot*) gene, the absence of which causes a severe increase in axonal off-track MTs and MT disorganisation (Alves-Silva et al., 2012; Qu et al., 2017; Sánchez-Soriano et al., 2009).

We first analysed potential mutual enhancement of *Efa6* and *shot* mutant phenotypes by determining numbers of MTs in axonal shaft filopodia: they were clearly elevated in the single mutant neurons (blue *vs.* orange bars in Fig.5F,G), which was substantially further increased in *shot^{3} Efa6$^{GX6[w-]}$* double mutant neurons (orange/blue bars in Fig. 5F,G). We then tested whether this increase in off-track MTs would correlate with more MT disorganisation. At 6 HIV, *shot^{3}* mutant neurons displayed a 2.4-fold increase in MDI (normalised to wild-type), slightly higher than the 1.55 fold measured in *Efa6$^{GX6[w-]}$* mutant neurons. This value was dramatically increased to 6.16 fold in *shot^{3} Efa6$^{GX6[w-]}$* double mutant neurons (orange and orange/blue columns in Fig. 7M), thus further suggesting that Efa6 and Shot perform complementary roles in regulating and maintaining axonal MTs and MT bundles.

Finally, we assessed whether these complementary relationships between Shot and Efa6 are relevant *in vivo*. Since complete loss of Shot is an embryonically lethal condition, we first asked whether the lack of just one copy of Shot has an enhancing effect on Efa6 deficiency. We first tested this in culture, by expressing *Efa6-RNAi* (blue bars in Fig.7L) in a *shot$^{3/+}$* heterozygous mutant background (orange bars in Fig.7L), and found at 6 HIV and 5 DIV that the combination of both genetic manipulations showed stronger MT disorganisation than the single mutant conditions. When testing the same genetic constellations in our optic lobe model, we found that the originally observed increase in MT disorganisations caused by cell-autonomous knock-down of *Efa6* (black arrows and blue bar in Fig.8B, E) was further enhanced when the same experiment was carried out in a *shot$^{3/+}$* heterozygous mutant background (black arrows and orange/blue bar in Fig.8C, E).

These findings further support our conclusion that there is a correlation between off-track MTs and MT disorganisation. Furthermore, they are consistent with a scenario where both Shot and Efa6 regulate axonal MTs but through independent and complementary pathways: Efa6 eliminates MTs at the cortex (with peripheral MTs persisting for longer if Efa6 is absent), whereas Shot actively maintains MTs in bundles (with more MTs going off-track if Shot is absent) - and both these functions complement each other during MT bundle maintenance (see further details in the Discussion).

Discussion

Cortical collapse factors are important microtubule regulators relevant for axon morphology

Axons are the structures that wire our brain and body and are therefore fundamental to nervous system function. To understand how axons are formed during development, maintained in a plastic state thereafter, and why they deteriorate in pathological conditions, we need to improve our knowledge of axonal cell biology (Hahn et al., 2019). The MT bundles that form the core of axons are an essential aspect of this cell biology, and understanding how these bundles are regulated and contribute to axon morphogenesis will provide essential insights into axon development and maintenance (Voelzmann et al., 2016a). Here we have addressed fundamental contributions made by cortical collapse factors. We started from reports that two such factors from distinct protein families both negatively impact on axon growth in species as diverse as *C. elegans* (*Ce*Efa6) and mouse (Kif21A; Chen et al., 2015; Chen et al., 2011; van der Vaart et al., 2013).

Here we now showed also for *Dm*Efa6 that it acts as a negative regulator of axon growth. As previously shown for *Ce*Efa6 (Chen et al., 2015; Chen et al., 2011; O'Rourke et al., 2010), we demonstrate that fly Efa6 is a cortical collapse factor, eliminating MTs primarily via the 18 aa long MTED as the only shared motif with *Ce*Efa6 in an otherwise entirely divergent N-terminus (Fig. 3C).

Capitalising on *Drosophila* neurons as a conceptually well-established model (Prokop et al., 2013; Voelzmann et al., 2016a), we went on to demonstrate two novel roles for Efa6: as a negative regulator of axon branching and a quality control factor maintaining MT bundle organisation. To perform these functions, Efa6 does not affect the dynamics of MTs contained within the central axonal bundles, but it eliminates mainly those MTs that leave these bundles (Fig.9A). By eliminating explorative MTs in GCs, it targets a key process underlying axon growth (yellow arrows in Fig.9C). By eliminating off-track MTs in the axon shaft it down-regulates the machinery seeding new interstitial branches (red arrow in Fig.9C), but also prevents these MTs from going astray and cause MT disorganisation (curled MTs in Fig.9C).

Therefore, our work provides conceptual understanding of cortical collapse factors, which can explain how their roles in subcellular MT regulation link to their reported axonal growth phenotypes during development and regeneration (Chen et al., 2015; Chen et al., 2011; Heidary et al., 2008; van der Vaart et al., 2013), and to their additional functions in axon branching and maintenance reported here. Apart from existing links of cortical collapse factors to neurodevelopmental disorders (Heidary et al., 2008; Tiab et al., 2004; van der Vaart et al., 2013), we would therefore predict future links also to neurodegeneration.

Roles of Efa6 during axonal growth

During axon growth, MTs constantly polymerise towards the periphery of GCs; many of these MTs are eliminated, and cortical collapse factors such as Efa6 appear to be essential for this. Only a fraction enters filopodia, potentially helped also by active guidance mechanisms mediated by MT-actin crosslinking through factors such as spectraplakins, tau or drebrin-Eb3 (Alves-Silva et al., 2012; Biswas and Kalil, 2018; Geraldo et al., 2008). The widely accepted protrusion-engorgement-consolidation model of axon growth proposes that stabilised MTs in filopodia can seed axon elongation events (Aletta and Greene, 1988; Goldberg and Burmeister, 1986; Prokop et al., 2013). This model is consistent with our findings for Efa6. Thus loss of Efa6 can contribute to enhanced axon growth in two ways: firstly, through allowing more MTs to enter filopodia; secondly, by allowing them to dwell in filopodia for longer thus enhancing the likelihood of their stabilisation (yellow arrows

in Fig.9C). This scenario can explain why loss of *Efa6* in *C. elegans* improves axon re-growth after injury and growth overshoot during development (Chen et al., 2015; Chen et al., 2011), and why the upregulation of Kif21A levels in GCs causes stalled axon growth (van der Vaart et al., 2013).

Roles of Efa6 during axonal branching

Axon branching can be induced either by GC splitting or through interstitial branch formation along the shaft, and both are likely to be influenced by Efa6. Branching through GC splitting occurs via parallel growth events seeded in the same GC (Acebes and Ferrus, 2000). This is expected to require simultaneous entry and stabilisation of more than one MT in different filopodia of the same growth cone (yellow arrows in Fig.9C); in the absence of Efa6 such coinciding events are far more likely to occur.

Current models of interstitial branching involve the active generation (e.g. through MT severing) and then stabilisation of off-track MTs that can seed new branches (Kalil and Dent, 2014; Lewis et al., 2013; Tymanskyj et al., 2017; Yu et al., 2008). This model fits with our observations in Efa6-deficient/over-expressing neurons: we find greater/lower numbers of MTs in shaft filopodia at 6 HIV, which then correlate with enhanced/reduced axonal branch numbers in mature neurons (red arrow in Fig.9C). Therefore, also interstitial branch formation is likely to be negatively regulated by *Efa6*.

This poses the question of whether interstitial branching requires active down-regulation of Efa6, either by physically removing it from future branching sites (Chen et al., 2015) or by switching its MT elimination function off. Potentially, no such regulation might be required, and the mere increase in off-track MTs generated by MT severing proteins (Yu et al., 2008) could be sufficient to outnumber Efa6-mediated elimination and induce branch formation (Fig.9D). Such a saturation model is supported by our experiments with *shot* (Fig.5F,G): filopodial MT numbers are elevated in *shot* mutant neurons although Efa6 is present under those conditions, suggesting that Efa6 function might be saturated by too many off-track MTs; but it functionally eliminates a fraction of these MTs as demonstrated by an additional increase in filopodial MT numbers in *shot Efa6* double-mutant neurons.

Roles of Efa6 during axonal MT bundle maintenance

Axonal MT disorganisation in Efa6-deficient neurons occurs gradually and can be induced even in mature neurons by knocking down Efa6 late (Fig.7K), arguing that Efa6 prevents MT disorganisation during axon development and maintenance, as is consistent with its continued expression in the nervous system (Fig.1). Such a continued role makes sense in a scenario where MT bundles remain highly dynamic and undergo polymerisation to drive renewal processes that prevent senescence (Hahn et al., 2019; Voelzmann et al., 2016a).

Based on these findings, we propose Efa6 to act as a quality control factor within our model of "local axon homeostasis" (Hahn et al., 2019; Voelzmann et al., 2016a). This model states that MTs in the force-enriched environment of axons have a tendency to go off-track and curl up (Pearce et al., 2018), thus potentially seeding MT disorganisation; different classes of MT-binding regulators prevent this by actively promoting the bundled conformation, with spectraplakins being the most prominent contributors (Voelzmann et al., 2017). Cortical collapse factors do not interfere with bundled MTs, but are ideally suited to contain the risk posed by occasional off-track MTs.

In this scenario, MTs are protected from cortical collapse as long as they are actively maintained in axonal bundles; this can explain the long known conundrum of how axonal MTs extend hundreds of micrometres in relative proximity to the cell cortex in axons, whereas in non-neuronal cells cortical

proximity of MTs tends to trigger either their elimination or tethered stabilisation (Fukata et al., 2002; Kaverina et al., 1998).

Evolutionary and mechanistic considerations of Efa6 function

We found that the MTED motif is a good predictor for MT elimination functions of Efa6 family members, whereas the rest of the N-terminus bears no obvious further reminiscence. This raises the question of how this motif eliminates MTs. So far, our various attempts with purified Efa6-Nterm::GFP or synthetic MTED::GFP revealed that they associate with MTs *in vitro* but failed to reconstitute any MT-eliminating activity (Fig. S8) - even when using *Xenopus* oocyte extracts to include the possibility that the small MTED acts indirectly as a co-factor or activity regulator of other proteins. Thus it could work through de-/polymerisers (e.g. kinesin-8 and -13, XMap215; Al-Bassam and Chang, 2011; Brouhard and Rice, 2014) or severers (McNally and Roll-Mecak, 2018; Sharp and Ross, 2012), but it could also block MT polymerisation processes by binding tubulins directly. In any case, the small size of MTEDs might come in handy as experimental tools to eliminate MTs, potentially displaying complementary properties to existing genetic tools such as the kinesin-13 Kif2C (Moore et al., 2005; Schimizzi et al., 2010), Stathmin (Marklund et al., 1996) or Spastin (Eckert et al., 2012).

Interestingly, the MT-eliminating role of Efa6 seems not to be conserved in chordates (Fig.2A). However, roles of cortical collapse factors in neurons seem to have been taken over by other proteins such as the kinesin-4 family member Kif21A (van der Vaart et al., 2013). The R954W mutation of Kif21A links to the eye movement disorder 'congenital fibrosis of extraocular muscles' (OMIM reference #135700; Tiab et al., 2004) and was shown to cause a shift of the protein's localisation in cultured hippocampal neurons from axons towards GCs, expected to cause loss of function in the axon shaft and gain of function in GCs (van der Vaart et al., 2013). The increased Kif21A levels in GCs correlate with reduced axon growth - and we observed the same with Efa6 over-expression (green bars in Fig.2D); the decreased levels of Kif21A in proximal axons correlate with a local increase in side branches - and we observed the same with Efa6 loss of function (blue bars in Fig.6E, L).

Finally, we found some indications that the C-terminal domains of Efa6 might display some degree of functional conservation. So far, work on mammalian PSDs has revealed functions for C-terminal domains in regulating ARF6, ARF1 or ARL14 during actin cytoskeletal reorganisation and membrane ruffling, tumour formation and immune regulation (Derrien et al., 2002; Paul et al., 2011; Pils et al., 2005). Our finding that PSD1 and C-terminal Efa6 constructs cause similar membrane ruffling phenotypes in fibroblasts (Figs.S4 and S6) suggests that some conserved functions reside in this region and might contribute, together with N-terminally mediated MT collapse, to the neuronal or non-neuronal defects that cause semi-lethality displayed by *Efa6* mutant flies (data not shown).

Conclusions and future perspectives

We propose that Efa6 acts as a cortical collapse factor which is important for the regulation of axonal MTs and relevant for axon growth, maintenance and branching. Although this function is evolutionarily not widely conserved, our findings provide a helpful paradigm for studies of other classes of cortical collapse factors also in mammalian neurons. Further important research avenues will be to identify the mechanism of Efa6-mediated MT elimination, not only to better understand how it can be regulated in axons but also to explore potential roles for MTEDs as molecular tools in cell biological research.

Acknowledgements

This work was made possible through support by the BBSRC to A.P (BB/I002448/1, BB/P020151/1, BB/L000717/1, BB/M007553/1) to N.S.S. (BB/M007456/1) and KD (BB/J005983/1), by parents as well as the Faculty of Life Sciences to Y.Q., by the Leverhulme Trust to I.H. (ECF-2017-247) and by the German Research Council (DFG) to A.V. (VO 2071/1-1). The Manchester Bioimaging Facility microscopes used in this study were purchased with grants from the BBSRC, The Wellcome Trust and The University of Manchester Strategic Fund. The Fly Facility has been supported by funds from The University of Manchester and the Wellcome Trust (087742/Z/08/Z). We thank Tom Millard and Marvin Bentley for very helpful comments on the manuscript, Simon Lowell for advice on the phylogenetic analyses, Hiro Ohkura for kindly providing DmEb1 antibody and Andrew Chisholm for the C.elegans Efa6 and human PSD constructs. Stocks obtained from the Bloomington *Drosophila* Stock Center (NIH P40OD018537) were used in this study.

References

Abascal, F., Zardoya, R., Posada, D. (2005). ProtTest: selection of best-fit models of protein evolution. *Bioinformatics* **21,** 2104-5 -- http://www.ncbi.nlm.nih.gov/pubmed/15647292

Acebes, A., Ferrus, A. (2000). Cellular and molecular features of axon collaterals and dendrites. *Trends Neurosci* **23,** 557-65 -- http://www.ncbi.nlm.nih.gov/pubmed/11074265

Adalbert, R., Coleman, M. P. (2012). Axon pathology in age-related neurodegenerative disorders. *Neuropathol Appl Neurobiol* **39,** 90–108 -- http://www.ncbi.nlm.nih.gov/pubmed/23046254

Adalbert, R., Nogradi, A., Babetto, E., Janeckova, L., Walker, S. A., Kerschensteiner, M., Misgeld, T., Coleman, M. P. (2009). Severely dystrophic axons at amyloid plaques remain continuous and connected to viable cell bodies. *Brain* **132,** 402-16 -- http://www.ncbi.nlm.nih.gov/pubmed/19059977

Al-Bassam, J., Chang, F. (2011). Regulation of microtubule dynamics by TOG-domain proteins XMAP215/Dis1 and CLASP. *Trends Cell Biol* **21,** 604-14 -- http://www.ncbi.nlm.nih.gov/pubmed/21782439

Aletta, J. M., Greene, L. A. (1988). Growth cone configuration and advance: a time-lapse study using video-enhanced differential interference contrast microscopy. *J Neurosci* **8,** 1425-35 -- http://www.ncbi.nlm.nih.gov/pubmed/3282037

Allan, V. J. (1993). Assay of membrane motility in interphase and metaphase Xenopus extracts. *Methods Cell Biol* **39,** 203-26 -- http://www.ncbi.nlm.nih.gov/pubmed/8246798

Allan, V. J., Vale, R. D. (1991). Cell cycle control of microtubule-based membrane transport and tubule formation in vitro. *J Cell Biol* **113,** 347-59 -- http://www.ncbi.nlm.nih.gov/pubmed/2010466

Alves-Silva, J., Sánchez-Soriano, N., Beaven, R., Klein, M., Parkin, J., Millard, T., Bellen, H., Venken, K. J. T., Ballestrem, C., Kammerer, R. A., Prokop, A. (2012). Spectraplakins promote microtubule-mediated axonal growth by functioning as structural microtubule-associated proteins and EB1-dependent +TIPs (Tip Interacting Proteins). *J. Neurosci* **32,** 9143-58 -- http://www.jneurosci.org/content/32/27/9143.full

Beaven, R., Dzhindzhev, N. S., Qu, Y., Hahn, I., Dajas-Bailador, F., Ohkura, H., Prokop, A. (2015). *Drosophila* CLIP-190 and mammalian CLIP-170 display reduced microtubule plus end association in the nervous system. *Mol Biol Cell* **26,** 1491-1508 -- http://www.molbiolcell.org/content/26/8/1491.abstract

Bernier, G., Kothary, R. (1998). Prenatal onset of axonopathy in Dystonia musculorum mice. *Dev Genet* **22,** 160-8 -- http://www.ncbi.nlm.nih.gov/entrez/query.fcgi?cmd=Retrieve&db=PubMed&dopt=Citation&list_uids=9581287

Bettencourt da Cruz, A., Schwarzel, M., Schulze, S., Niyyati, M., Heisenberg, M., Kretzschmar, D. (2005). Disruption of the MAP1B-related protein FUTSCH leads to changes in the neuronal cytoskeleton, axonal transport defects, and progressive neurodegeneration in *Drosophila*. *Mol Biol Cell* **16,** 2433-42 -- http://www.ncbi.nlm.nih.gov/entrez/query.fcgi?cmd=Retrieve&db=PubMed&dopt=Citation&list_uids=15772149

Biswas, S., Kalil, K. (2018). The microtubule-associated protein tau mediates the organization of microtubules and their dynamic exploration of actin-rich lamellipodia and filopodia of cortical growth cones. *J Neurosci* **38,** 291-307 -- http://www.ncbi.nlm.nih.gov/pubmed/29167405

Brouhard, G. J., Rice, L. M. (2014). The contribution of aß-tubulin curvature to microtubule dynamics. *J Cell Biol* **207,** 323-34 -- http://www.ncbi.nlm.nih.gov/pubmed/25385183

Calkins, D. J. (2013). Age-Related Changes in the Visual Pathways: Blame It on the AxonAge-Related Changes in the Visual Pathways. *Investigative Ophthalmology & Visual Science* **54,** ORSF37-ORSF41 -- https://dx.doi.org/10.1167/iovs.13-12784

Chen, L., Chuang, M., Koorman, T., Boxem, M., Jin, Y., Chisholm, A. D. (2015). Axon injury triggers EFA-6 mediated destabilization of axonal microtubules via TACC and doublecortin like kinase. *eLife* **4,** e08695 -- https://elifesciences.org/articles/08695

Chen, L., Wang, Z., Ghosh-Roy, A., Hubert, T., Yan, D., O'Rourke, S., Bowerman, B., Wu, Z., Jin, Y., Chisholm, A. D. (2011). Axon regeneration pathways identified by systematic genetic screening in *C. elegans*. *Neuron* **71,** 1043-57 -- http://www.ncbi.nlm.nih.gov/pubmed/21943602

Crooks, G. E., Hon, G., Chandonia, J. M., Brenner, S. E. (2004). WebLogo: a sequence logo generator. *Genome Res* **14,** 1188-90 -- http://www.ncbi.nlm.nih.gov/pubmed/15173120

D'Souza-Schorey, C., Chavrier, P. (2006). ARF proteins: roles in membrane traffic and beyond. *Nature Rev Molec Cell Biol* **7,** 347 -- http://dx.doi.org/10.1038/nrm1910

Dalpe, G., Leclerc, N., Vallee, A., Messer, A., Mathieu, M., De Repentigny, Y., Kothary, R. (1998). Dystonin is essential for maintaining neuronal cytoskeleton organization. *Mol Cell Neurosci* **10,** 243-57 -- http://www.ncbi.nlm.nih.gov/entrez/query.fcgi?cmd=Retrieve&db=PubMed&dopt=Citation&list_uids=9604204

Darriba, D., Taboada, G. L., Doallo, R., Posada, D. (2011). ProtTest 3: fast selection of best-fit models of protein evolution. *Bioinformatics* **27,** 1164-5 -- http://www.ncbi.nlm.nih.gov/pubmed/21335321

Debanne, D., Campanac, E., Bialowas, A., Carlier, E., Alcaraz, G. (2011). Axon physiology. *Physiol Rev* **91,** 555-602 -- http://www.ncbi.nlm.nih.gov/pubmed/21527732

Dent, E. W., Gupton, S. L., Gertler, F. B. (2011). The growth cone cytoskeleton in axon outgrowth and guidance. *Cold Spring Harb Perspect Biol* **3,** a001800 -- http://www.ncbi.nlm.nih.gov/entrez/query.fcgi?cmd=Retrieve&db=PubMed&dopt=Citation&list_uids=21106647

Derrien, V., Couillault, C., Franco, M., Martineau, S., Montcourrier, P., Houlgatte, R., Chavrier, P. (2002). A conserved C-terminal domain of EFA6-family ARF6-guanine nucleotide exchange factors induces lengthening of microvilli-like membrane protrusions. *J Cell Sci* **115,** 2867-79 -- http://www.ncbi.nlm.nih.gov/pubmed/12082148

Eckert, T., Le, D. T.-V., Link, S., Friedmann, L., Woehlke, G. (2012). Spastin's microtubule-binding properties and comparison to katanin. *PLoS One* **7,** e50161 -- https://doi.org/10.1371/journal.pone.0050161

Elliott, S. L., Cullen, C. F., Wrobel, N., Kernan, M. J., Ohkura, H. (2005). EB1 is essential during *Drosophila* development and plays a crucial role in the integrity of chordotonal mechanosensory organs. *Mol Biol Cell* **16,** 891-901 -- http://www.ncbi.nlm.nih.gov/entrez/query.fcgi?cmd=Retrieve&db=PubMed&dopt=Citation&list_uids=15591130

Fang, Y., Bonini, N. M. (2012). Axon degeneration and regeneration: insights from *Drosophila* models of nerve injury. *Annu Rev Cell Dev Biol* **28,** 575-97 -- http://www.ncbi.nlm.nih.gov/pubmed/22831639

Fassier, C., Tarrade, A., Peris, L., Courageot, S., Mailly, P., Dalard, C., Delga, S., Roblot, N., Lefevre, J., Job, D., Hazan, J., Curmi, P. A., Melki, J. (2013). Microtubule-targeting drugs rescue axonal swellings in cortical neurons from spastin knockout mice. *Dis Model Mech* **6,** 72-83 -- http://www.ncbi.nlm.nih.gov/pubmed/22773755

Fiala, J. C., Feinberg, M., Peters, A., Barbas, H. (2007). Mitochondrial degeneration in dystrophic neurites of senile plaques may lead to extracellular deposition of fine filaments. *Brain Struct Funct* **212,** 195-207 -- http://www.ncbi.nlm.nih.gov/entrez/query.fcgi?cmd=Retrieve&db=PubMed&dopt=Citation&list_uids=17717688

Franco, M., Peters, P. J., Boretto, J., van Donselaar, E., Neri, A., D'Souza-Schorey, C., Chavrier, P. (1999). EFA6, a sec7 domain-containing exchange factor for ARF6, coordinates membrane recycling and actin cytoskeleton organization. *EMBO J* **18,** 1480-91 -- http://www.ncbi.nlm.nih.gov/pubmed/10075920

Fukata, M., Watanabe, T., Noritake, J., Nakagawa, M., Yamaga, M., Kuroda, S., Matsuura, Y., Iwamatsu, A., Perez, F., Kaibuchi, K. (2002). Rac1 and Cdc42 capture microtubules through IQGAP1 and CLIP-170. *Cell* **109,** 873–885 -- https://doi-org.manchester.idm.oclc.org/10.1016/S0092-8674(02)00800-0

Geraldo, S., Khanzada, U. K., Parsons, M., Chilton, J. K., Gordon-Weeks, P. R. (2008). Targeting of the F-actin-binding protein drebrin by the microtubule plus-tip protein EB3 is required for neuritogenesis. *Nat Cell Biol* **10,** 1181-9 -- http://www.ncbi.nlm.nih.gov/entrez/query.fcgi?cmd=Retrieve&db=PubMed&dopt=Citation&list_uids=18806788

Goldberg, D. J., Burmeister, D. W. (1986). Stages in axon formation: observations of growth of *Aplysia* axons in culture using video-enhanced contrast-differential interference contrast microscopy. *J Cell Biol* **103,** 1921-31 -- http://www.ncbi.nlm.nih.gov/pubmed/3782290

Goujon, M., McWilliam, H., Li, W., Valentin, F., Squizzato, S., Paern, J., Lopez, R. (2010). A new bioinformatics analysis tools framework at EMBL-EBI. *Nucleic Acids Res* **38,** W695-9 -- http://www.ncbi.nlm.nih.gov/pubmed/20439314

Grieder, N. C., de Cuevas, M., Spradling, A. C. (2000). The fusome organizes the microtubule network during oocyte differentiation in *Drosophila*. *Development* **127,** 4253-4264 -- http://dev.biologists.org/content/127/19/4253

Hahn, I., Fuss, B., Peters, A., Werner, T., Sieberg, A., Gosejacob, D., Hoch, M. (2013). The *Drosophila* Arf GEF Steppke controls MAPK activation in EGFR signaling. *J Cell Sci* **126,** 2470-9 -- http://www.ncbi.nlm.nih.gov/pubmed/23549788

Hahn, I., Voelzmann, A., Liew, Y.-T., Costa-Gomes, B., Prokop, A. (2019). The model of local axon homeostasis - explaining the role and regulation of microtubule bundles in axon maintenance and pathology. *bioRxiv***,** 10.1101/577320 -- https://www.biorxiv.org/content/10.1101/577320v2

Han, M. V., Zmasek, C. M. (2009). phyloXML: XML for evolutionary biology and comparative genomics. *BMC Bioinformatics* **10,** 356 -- http://www.ncbi.nlm.nih.gov/pubmed/19860910

Hancock, J. F., Cadwallader, K., Paterson, H., Marshall, C. J. (1991). A CAAX or a CAAL motif and a second signal are sufficient for plasma membrane targeting of ras proteins. *EMBO J* **10,** 4033-9 -- http://www.ncbi.nlm.nih.gov/pubmed/1756714

Hassan, B. A., Bermingham, N. A., He, Y., Sun, Y., Jan, Y. N., Zoghbi, H. Y., Bellen, H. J. (2000). *atonal* regulates neurite arborization but does not act as a proneural gene in the *Drosophila* brain. *Neuron* **25,** 549-61 -- http://www.ncbi.nlm.nih.gov/entrez/query.fcgi?cmd=Retrieve&db=PubMed&dopt=Citation&list_uids=10774724

Heasman, J. (2006). Patterning the early Xenopus embryo. *Development* **133,** 1205-17 -- http://www.ncbi.nlm.nih.gov/pubmed/16527985

Heidary, G., Engle, E. C., Hunter, D. G. (2008). Congenital Fibrosis of the Extraocular Muscles. *Seminars in Ophthalmology* **23,** 3-8 -- https://doi.org/10.1080/08820530701745181

Helenius, J., Brouhard, G., Kalaidzidis, Y., Diez, S., Howard, J. (2006). The depolymerizing kinesin MCAK uses lattice diffusion to rapidly target microtubule ends. *Nature* **441,** 115-9 -- http://www.ncbi.nlm.nih.gov/pubmed/16672973

Hinrichs, M. H., Jalal, A., Brenner, B., Mandelkow, E., Kumar, S., Scholz, T. (2012). Tau protein diffuses along the microtubule lattice. *J Biol Chem* **287,** 38559-68 -- http://www.ncbi.nlm.nih.gov/pubmed/23019339

Honnappa, S., Gouveia, S. M., Weisbrich, A., Damberger, F. F., Bhavesh, N. S., Jawhari, H., Grigoriev, I., van Rijssel, F. J., Buey, R. M., Lawera, A., Jelesarov, I., Winkler, F. K., Wuthrich, K., Akhmanova, A., Steinmetz, M. O. (2009). An EB1-binding motif acts as a microtubule tip localization signal. *Cell* **138,** 366-76 -- http://www.ncbi.nlm.nih.gov/entrez/query.fcgi?cmd=Retrieve&db=PubMed&dopt=Citation&list_uids=19632184

Huang, J., Zhou, W., Dong, W., Watson, A. M., Hong, Y. (2009). From the Cover: Directed, efficient, and versatile modifications of the *Drosophila* genome by genomic engineering. *Proc Natl Acad Sci U S A* **106,** 8284-9 -- http://www.ncbi.nlm.nih.gov/pubmed/19429710

Kalil, K., Dent, E. W. (2014). Branch management: mechanisms of axon branching in the developing vertebrate CNS. *Nat Rev Neurosci* **15,** 7-18 -- http://www.ncbi.nlm.nih.gov/pubmed/24356070

Kaverina, I., Rottner, K., Small, J. V. (1998). Targeting, capture, and stabilization of microtubules at early focal adhesions. *J Cell Biol* **142,** 181-90 -- http://www.ncbi.nlm.nih.gov/pubmed/9660872

Kolodziej, P. A., Jan, L. Y., Jan, Y. N. (1995). Mutations that affect the length, fasciculation, or ventral orientation of specific sensory axons in the *Drosophila* embryo. *Neuron* **15,** 273-286 -- https://doi-org.manchester.idm.oclc.org/10.1016/0896-6273(95)90033-0

Krieg, M., Stühmer, J., Cueva, J. G., Fetter, R., Spilker, K., Cremers, D., Shen, K., Dunn, A. R., Goodman, M. B. (2017). Genetic defects in β-spectrin and tau sensitize *C. elegans* axons to movement-induced damage via torque-tension coupling. *Elife* **6,** e20172 -- https://doi.org/10.7554/eLife.20172

Küppers-Munther, B., Letzkus, J., Lüer, K., Technau, G., Schmidt, H., Prokop, A. (2004). A new culturing strategy optimises *Drosophila* primary cell cultures for structural and functional analyses. *Dev. Biol.* **269,** 459-478 -- http://www.ncbi.nlm.nih.gov/entrez/query.fcgi?cmd=Retrieve&db=PubMed&dopt=Citation&list_uids=15110713

Lewis, T. L., Jr., Courchet, J., Polleux, F. (2013). Cell biology in neuroscience: Cellular and molecular mechanisms underlying axon formation, growth, and branching. *J Cell Biol* **202,** 837-48 -- http://www.ncbi.nlm.nih.gov/pubmed/24043699

Lowery, L. A., van Vactor, D. (2009). The trip of the tip: understanding the growth cone machinery. *Nat Rev Mol Cell Biol* **10,** 332-43 -- http://www.ncbi.nlm.nih.gov/entrez/query.fcgi?cmd=Retrieve&db=PubMed&dopt=Citation&list_uids=19373241

Luo, L., Liao, Y. J., Jan, L. Y., Jan, Y. N. (1994). Distinct morphogenetic functions of similar small GTPases: *Drosophila* Drac1 is involved in axonal outgrowth and myoblast fusion. *Genes Dev.* **8,** 1787-1802 -- http://www.ncbi.nlm.nih.gov/entrez/query.fcgi?cmd=Retrieve&db=PubMed&dopt=Citation&list_uids=7958857

Macia, E., Partisani, M., Favard, C., Mortier, E., Zimmermann, P., Carlier, M. F., Gounon, P., Luton, F., Franco, M. (2008). The pleckstrin homology domain of the Arf6-specific exchange factor EFA6 localizes to the plasma membrane by interacting with phosphatidylinositol 4,5-bisphosphate and F-actin. *J Biol Chem* **283,** 19836-44 -- http://www.ncbi.nlm.nih.gov/pubmed/18490450

Marklund, U., Larsson, N., Gradin, H. M., Brattsand, G., Gullberg, M. (1996). Oncoprotein 18 is a phosphorylation-responsive regulator of microtubule dynamics. *EMBO J* **15,** 5290-8 -- http://www.ncbi.nlm.nih.gov/pubmed/8895574

Marner, L., Nyengaard, J. R., Tang, Y., Pakkenberg, B. (2003). Marked loss of myelinated nerve fibers in the human brain with age. *J Comp Neurol* **462,** 144-52 -- http://www.ncbi.nlm.nih.gov/pubmed/12794739

McNally, F. J., Roll-Mecak, A. (2018). Microtubule-severing enzymes: From cellular functions to molecular mechanism. *J Cell Biol* **217,** 4057-69 -- http://jcb.rupress.org/content/early/2018/10/31/jcb.201612104

McWilliam, H., Li, W., Uludag, M., Squizzato, S., Park, Y. M., Buso, N., Cowley, A. P., Lopez, R. (2013). Analysis Tool Web Services from the EMBL-EBI. *Nucleic Acids Res* **41,** W597-600 -- http://www.ncbi.nlm.nih.gov/pubmed/23671338

Medana, I. M., Esiri, M. M. (2003). Axonal damage: a key predictor of outcome in human CNS diseases. *Brain* **126,** 515-30 -- http://www.ncbi.nlm.nih.gov/pubmed/12566274

Moore, A. T., Rankin, K. E., von Dassow, G., Peris, L., Wagenbach, M., Ovechkina, Y., Andrieux, A., Job, D., Wordeman, L. (2005). MCAK associates with the tips of polymerizing microtubules. *J Cell Biol* **169,** 391-397 -- http://jcb.rupress.org/content/jcb/169/3/391.full.pdf

O'Rourke, S. M., Christensen, S. N., Bowerman, B. (2010). *Caenorhabditis elegans* EFA-6 limits microtubule growth at the cell cortex. *Nat Cell Biol* **12,** 1235-41 -- http://www.ncbi.nlm.nih.gov/entrez/query.fcgi?cmd=Retrieve&db=PubMed&dopt=Citation&list_uids=21076413

Patel, J. T., Belsham, H. R., Rathbone, A. J., Wickstead, B., Gell, C., Friel, C. T. (2016). The family-specific alpha4-helix of the kinesin-13, MCAK, is critical to microtubule end recognition. *Open Biol* **6** -- http://www.ncbi.nlm.nih.gov/pubmed/27733589

Paul, P., van den Hoorn, T., Jongsma, Marlieke L. M., Bakker, Mark J., Hengeveld, R., Janssen, L., Cresswell, P., Egan, David A., van Ham, M., ten Brinke, A., Ovaa, H., Beijersbergen, Roderick L., Kuijl, C., Neefjes, J. (2011). A Genome-wide Multidimensional RNAi Screen Reveals Pathways Controlling MHC Class II Antigen Presentation. *Cell* **145,** 268-283 -- http://dx.doi.org/10.1016/j.cell.2011.03.023

Pearce, S. P., Heil, M., Jensen, O. E., Jones, G. W., Prokop, A. (2018). Curvature-sensitive kinesin binding can explain microtubule ring formation and reveals chaotic dynamics in a mathematical model. *Bull Math Biol* **80,** 3002-22 -- https://tinyurl.com/yd43ncb9

Pils, D., Horak, P., Gleiss, A., Sax, C., Fabjani, G., Moebus, V. J., Zielinski, C., Reinthaller, A., Zeillinger, R., Krainer, M. (2005). Five genes from chromosomal band 8p22 are significantly down-regulated in ovarian carcinoma. *Cancer* **104,** 2417-2429 -- http://dx.doi.org/10.1002/cncr.21538

Ponting, C. P., Phillips, C., Davies, K. E., Blake, D. J. (1997). PDZ domains: targeting signalling molecules to sub-membranous sites. *Bioessays* **19,** 469-79 -- http://www.ncbi.nlm.nih.gov/pubmed/9204764

Prokop, A. (2013a). The intricate relationship between microtubules and their associated motor proteins during axon growth and maintenance. *Neur Dev* **8,** 17 -- http://www.neuraldevelopment.com/content/8/1/17

Prokop, A. (2013b). A rough guide to *Drosophila* mating schemes. *figshare*, dx.doi.org/10.6084/m9.figshare.106631 -- http://dx.doi.org/10.6084/m9.figshare.106631

Prokop, A. (2016). Fruit flies in biological research. *Biological Sciences Review* **28,** 10-14 -- https://tinyurl.com/ybvpoqmw

Prokop, A., Beaven, R., Qu, Y., Sánchez-Soriano, N. (2013). Using fly genetics to dissect the cytoskeletal machinery of neurons during axonal growth and maintenance. *J. Cell Sci.* **126,** 2331-41 -- http://dx.doi.org/10.1242/jcs.126912

Prokop, A., Küppers-Munther, B., Sánchez-Soriano, N. (2012). Using primary neuron cultures of *Drosophila* to analyse neuronal circuit formation and function. *In* "The making and un-making of neuronal circuits in *Drosophila*" (B. A. Hassan, Ed.), Vol. 69, pp. 225-47. Humana Press, New York -- http://dx.doi.org/10.1007/978-1-61779-830-6_10

Prokop, A., Meinertzhagen, I. A. (2006). Development and structure of synaptic contacts in *Drosophila*. *Semin Cell Dev Biol* **17,** 20-30 -- http://www.ncbi.nlm.nih.gov/entrez/query.fcgi?cmd=Retrieve&db=PubMed&dopt=Citation&list_uids=16384719

Qu, Y., Hahn, I., Webb, S. E. D., Pearce, S. P., Prokop, A. (2017). Periodic actin structures in neuronal axons are required to maintain microtubules. *Mol Biol Cell* **28** 296-308 -- http://www.molbiolcell.org/content/early/2016/11/21/mbc.E16-10-0727

Rogers, S. L., Rogers, G. C., Sharp, D. J., Vale, R. D. (2002). *Drosophila* EB1 is important for proper assembly, dynamics, and positioning of the mitotic spindle. *J Cell Biol* **158,** 873-84 -- http://www.ncbi.nlm.nih.gov/entrez/query.fcgi?cmd=Retrieve&db=PubMed&dopt=Citation&list_uids=12213835

Ronquist, F., Teslenko, M., van der Mark, P., Ayres, D. L., Darling, A., Hohna, S., Larget, B., Liu, L., Suchard, M. A., Huelsenbeck, J. P. (2012). MrBayes 3.2: efficient Bayesian phylogenetic inference and model choice across a large model space. *Syst Biol* **61,** 539-42 -- http://www.ncbi.nlm.nih.gov/pubmed/22357727

Sánchez-Soriano, N., Gonçalves-Pimentel, C., Beaven, R., Haessler, U., Ofner, L., Ballestrem, C., Prokop, A. (2010). *Drosophila* growth cones: a genetically tractable platform for the analysis of axonal growth dynamics. *Dev. Neurobiol.* **70,** 58-71 -- https://onlinelibrary.wiley.com/doi/abs/10.1002/dneu.20762

Sánchez-Soriano, N., Travis, M., Dajas-Bailador, F., Goncalves-Pimentel, C., Whitmarsh, A. J., Prokop, A. (2009). Mouse ACF7 and *Drosophila* Short stop modulate filopodia formation and microtubule organisation during neuronal growth. *J Cell Sci* **122,** 2534-42 -- http://jcs.biologists.org/content/122/14/2534.long

Schimizzi, G. V., Currie, J. D., Rogers, S. L. (2010). Expression levels of a kinesin-13 microtubule depolymerase modulates the effectiveness of anti-microtubule agents. *PLoS One* **5,** e11381 -- https://doi.org/10.1371/journal.pone.0011381

Schindelin, J., Arganda-Carreras, I., Frise, E., Kaynig, V., Longair, M., Pietzsch, T., Preibisch, S., Rueden, C., Saalfeld, S., Schmid, B., Tinevez, J. Y., White, D. J., Hartenstein, V., Eliceiri, K., Tomancak, P., Cardona, A. (2012). Fiji: an open-source platform for biological-image analysis. *Nat Methods* **9,** 676-82 -- http://www.ncbi.nlm.nih.gov/pubmed/22743772

Seibel, N. M., Eljouni, J., Nalaskowski, M. M., Hampe, W. (2007). Nuclear localization of enhanced green fluorescent protein homomultimers. *Analytical Biochemistry* **368,** 95-99 -- http://www.sciencedirect.com/science/article/pii/S0003269707003399

Sharp, D. J., Ross, J. L. (2012). Microtubule-severing enzymes at the cutting edge. *J Cell Sci* **125,** 2561-9 -- http://www.ncbi.nlm.nih.gov/pubmed/22595526

Sievers, F., Wilm, A., Dineen, D., Gibson, T. J., Karplus, K., Li, W., Lopez, R., McWilliam, H., Remmert, M., Soding, J., Thompson, J. D., Higgins, D. G. (2011). Fast, scalable generation of

high-quality protein multiple sequence alignments using Clustal Omega. *Mol Syst Biol* **7,** 539 -- http://www.ncbi.nlm.nih.gov/pubmed/21988835

Stefana, M. I., Driscoll, P. C., Obata, F., Pengelly, A. R., Newell, C. L., MacRae, J. I., Gould, A. P. (2017). Developmental diet regulates *Drosophila* lifespan via lipid autotoxins. *Nat Commun* **8,** 1384 -- http://www.ncbi.nlm.nih.gov/pubmed/29123106

Tarrade, A., Fassier, C., Courageot, S., Charvin, D., Vitte, J., Peris, L., Thorel, A., Mouisel, E., Fonknechten, N., Roblot, N., Seilhean, D., Dierich, A., Hauw, J. J., Melki, J. (2006). A mutation of spastin is responsible for swellings and impairment of transport in a region of axon characterized by changes in microtubule composition. *Hum Mol Genet* **15,** 3544-58 -- http://www.ncbi.nlm.nih.gov/pubmed/17101632

Tiab, L., Manzi, V. d. A., Borruat, F.-X., Munier, F., Schorderet, D. (2004). Mutation analysis of KIF21A in congenital fibrosis of the extraocular muscles (CFEOM) patients. *Ophthalmic Genetics* **25,** 241-246 -- https://doi.org/10.1080/13816810490902828

Tymanskyj, S. R., Yang, B., Falnikar, A., Lepore, A. C., Ma, L. (2017). MAP7 regulates axon collateral branch development in dorsal root ganglion neurons. *J Neurosci* **37,** 1648-1661 -- http://www.ncbi.nlm.nih.gov/pubmed/28069923

Vale, R. D., Toyoshima, Y. Y. (1988). Rotation and translocation of microtubules in vitro induced by dyneins from *Tetrahymena* cilia. *Cell* **52,** 459-69 -- http://www.ncbi.nlm.nih.gov/pubmed/2964278

van der Vaart, B., van Riel, Wilhelmina E., Doodhi, H., Kevenaar, Josta T., Katrukha, Eugene A., Gumy, L., Bouchet, Benjamin P., Grigoriev, I., Spangler, Samantha A., Yu, Ka L., Wulf, Phebe S., Wu, J., Lansbergen, G., van Battum, Eljo Y., Pasterkamp, R. J., Mimori-Kiyosue, Y., Demmers, J., Olieric, N., Maly, Ivan V., Hoogenraad, Casper C., Akhmanova, A. (2013). CFEOM1-associated kinesin KIF21A is a cortical microtubule growth inhibitor. *Developmental Cell* **27,** 145-160 -- http://dx.doi.org/10.1016/j.devcel.2013.09.010

Voelzmann, A., Hahn, I., Pearce, S., Sánchez-Soriano, N. P., Prokop, A. (2016a). A conceptual view at microtubule plus end dynamics in neuronal axons. *Brain Res Bulletin* **126,** 226-37 -- http://www.sciencedirect.com/science/article/pii/S0361923016301885

Voelzmann, A., Liew, Y.-T., Qu, Y., Hahn, I., Melero, C., Sánchez-Soriano, N., Prokop, A. (2017). *Drosophila* Short stop as a paradigm for the role and regulation of spectraplakins. *Sem Cell Dev Biol* **69,** 40-57 -- http://www.sciencedirect.com/science/article/pii/S1084952117302124

Voelzmann, A., Okenve-Ramos, P., Qu, Y., Chojnowska-Monga, M., del Caño-Espinel, M., Prokop, A., Sánchez-Soriano, N. (2016b). Tau and spectraplakins promote synapse formation and maintenance through Jun kinase and neuronal trafficking. *eLife* **5,** e14694 -- https://elifesciences.org/content/5/e14694

Wang, J. T., Medress, Z. A., Barres, B. A. (2012). Axon degeneration: molecular mechanisms of a self-destruction pathway. *J Cell Biol* **196,** 7-18 -- http://www.ncbi.nlm.nih.gov/pubmed/22232700

Yu, W., Qiang, L., Solowska, J. M., Karabay, A., Korulu, S., Baas, P. W. (2008). The microtubule-severing proteins spastin and katanin participate differently in the formation of axonal branches. *Mol Biol Cell* **19,** 1485-98 -- http://www.ncbi.nlm.nih.gov/entrez/query.fcgi?cmd=Retrieve&db=PubMed&dopt=Citation&list_uids=18234839

Zeidler, M. P., Tan, C., Bellaiche, Y., Cherry, S., Hader, S., Gayko, U., Perrimon, N. (2004). Temperature-sensitive control of protein activity by conditionally splicing inteins. *Nat Biotech* **22,** 871-876 -- http://dx.doi.org/10.1038/nbt979

Zschätzsch, M., Oliva, C., Langen, M., De Geest, N., Ozel, M. N., Williamson, W. R., Lemon, W. C., Soldano, A., Munck, S., Hiesinger, P. R., Sánchez-Soriano, N., Hassan, B. A. (2014). Regulation of branching dynamics by axon-intrinsic asymmetries in Tyrosine Kinase Receptor signaling. *Elife* **3,** e01699 -- http://www.ncbi.nlm.nih.gov/pubmed/24755286

Figures

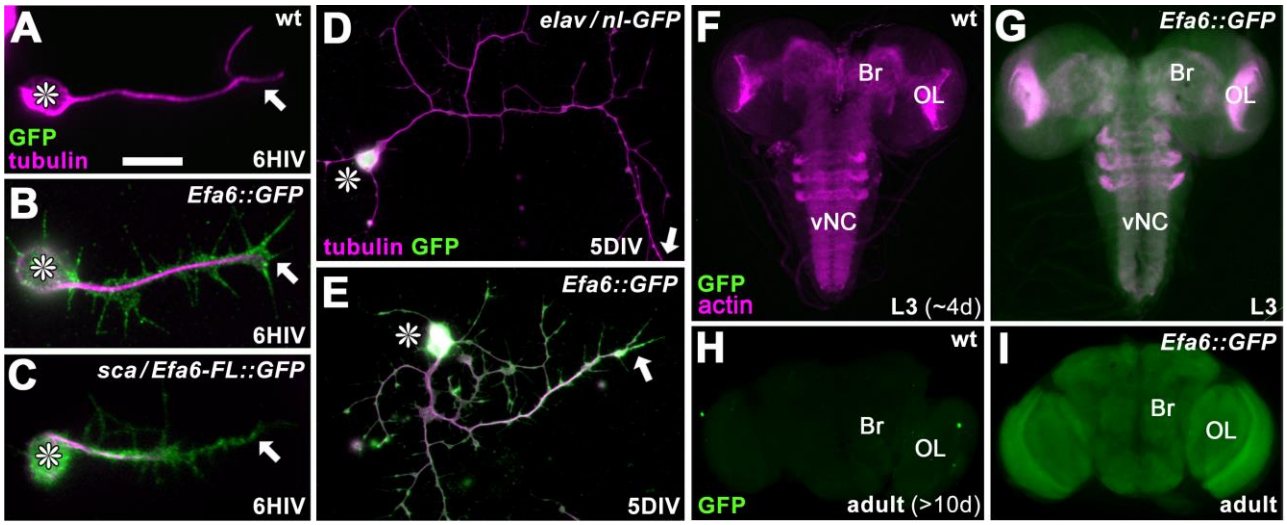

Fig. 1 Efa6 is expressed throughout neurons at all developmental stages. **A-E)** Images of primary *Drosophila* neurons at 6HIV or 5DIV (at indicated bottom right), stained for tubulin (magenta) and GFP (green); control neurons are wild-type (wt) or express *elav-Gal4*-driven nuclear GFP (*elav / nl-GFP*), whereas further neurons are either derived from the endogenously tagged Efa6::GFP line or express Efa6-FL::GFP under the control of sca-Gal4 (*sca / Efa6-FL::GFP*); asterisks indicate cell bodies and arrow the axon tips. **F-I)** Late larval CNSs at about 4d of development from egg lay (L3; F,G) and adult CNSs from 10d old flies (H,I) derived from control wild-type animals (wt) or the Efa6::GFP line (*Efa6::GFP*), stained for GFP and actin (Phalloidin, only larval preparations); OL, optic lobe; Br, central brain; vNC, ventral nerve cord. Scale bar in A represent 15µm in A-C, 25µm in D and E, 75µm in F and G, 130µm in H and I.

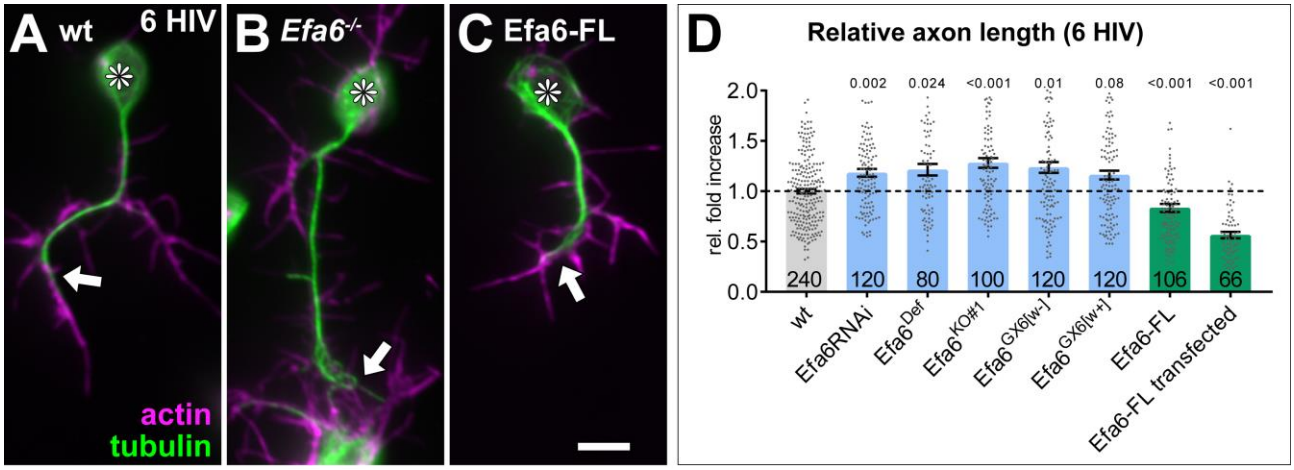

Fig. 2. Efa6 regulates axonal length in primary *Drosophila* neurons. **A-C)** Examples of primary *Drosophila* neurons at 6HIV, all stained for actin (magenta) and tubulin (green); neurons are either wild-type controls (A), Efa6-deficient (B), expressing Efa6-FL::GFP (C); asterisks indicate cell bodies, arrows point at axon tips; the scale bar in C represents 10µm. **D)** Quantification of axon lengths at 6HIV; different genotypes are colour-coded: grey, wild-type controls; blue, different *Efa6* loss-of-function conditions; green, neurons over-expressing Efa6 variants; data represent fold-change relative to wild-type controls (indicated as horizontal dashed "ctrl" line); they are shown as single data points and a bar indicating mean ± SEM data; P values from Mann-Whitney tests are given above each column, sample numbers at the bottom of each bar. For raw data see T2, which can be downloaded here: www.prokop.co.uk/Qu+al/RawData.zip.

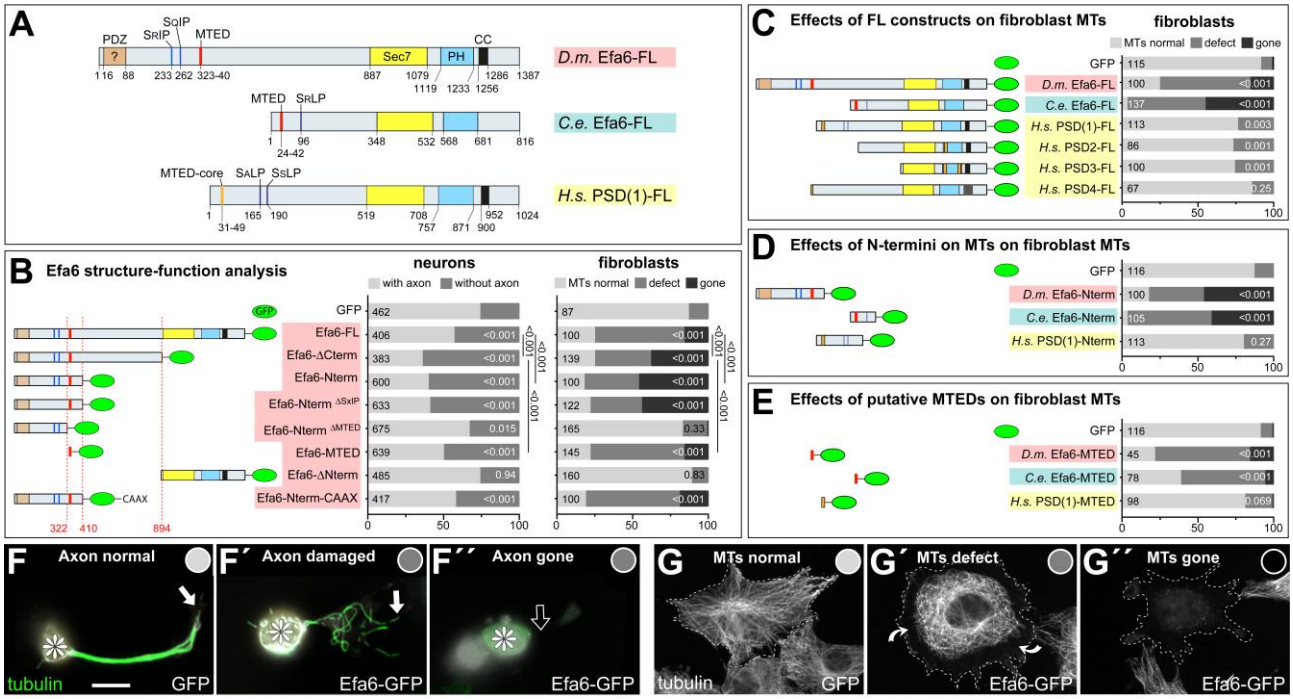

Fig. 3. Efa6 domain and motif requirements for MT elimination in neurons and fibroblasts. **A)** Schematics of *Drosophila melanogaster (Dm)* Efa6 (isoform C, CG31158), *Caenorhabditis elegans (Ce)* Efa6 (isoform Y55D9A.1a) and *Homo sapiens* (human) PSD1 (isoform 201/202, NP_002770.3), illustrating the positions (numbers indicate first and last residues) of the putative PSD95-Dlg1-ZO1 domain [PDZ; expected to anchor to transmembrane proteins (Ponting et al., 1997), but not mediating obvious membrane association in fibroblasts: Figs.S4C,D, 6C), SxIP/SxLP motifs (SRIP, SQIP, SALP, SSLP), the MT-binding domain (MTED), SEC7 domain, plekstrin homology (PH) domain and coiled-coil domain (CC). **B)** Schematics on the left follow the same colour code and show the *Dm*Efa6 constructs used in this study (dashed red lines indicate the last/first residue before/behind the truncation). Bar graphs on the right show the impact that transfection of these constructs had on axon loss in primary *Drosophila* neurons (dark grey in left graph) and on MT loss in fibroblasts (dark grey or black as indicated; for respective images see F and G below). **C-E)** Analogous fibroblast experiments as performed with *Drosophila* constructs were performed with full length constructs of *C. elegans* Efa6 and human PSDs (C), with N-terminal constructs (D) or synthetic MTEDs (E) of *Dm* and *Ce*Efa6 and of human PSD1. Throughout this figure, construct names are highlighted in red for *Drosophila*, light blue for *C. elegans* and yellow for *Homo sapiens*; all graph bars indicate percentages of neurons with/without axons (light/dark grey) and of fibroblasts with normal, reduced or absent MTs (light, medium, dark grey, respectively); numbers in the left end of each bar indicate sample numbers; numbers in the right end represent P values from Chi^2 tests relative to GFP controls, and additional numbers and black bars in B provide further statistical comparisons. **F-F'')** Primary neurons expressing Efa6-FL::GFP transgenically and stained for tubulin (asterisks, cell bodies; white arrows, axon tips; open arrow, absent axon). **G-G")** Fibroblasts expressing Efa6-FL::GFP and stained for tubulin; curved arrows indicate areas where MTs are retracted from the cell periphery; grey dots in F-G" indicate the phenotypic categories for each neuron and fibroblasts, as used for quantitative analyses in the graphs above. Scale bar at bottom of F refers to 10µm in F and 25µm in G. For raw data see T3, which can be downloaded here: www.prokop.co.uk/Qu+al/RawData.zip.

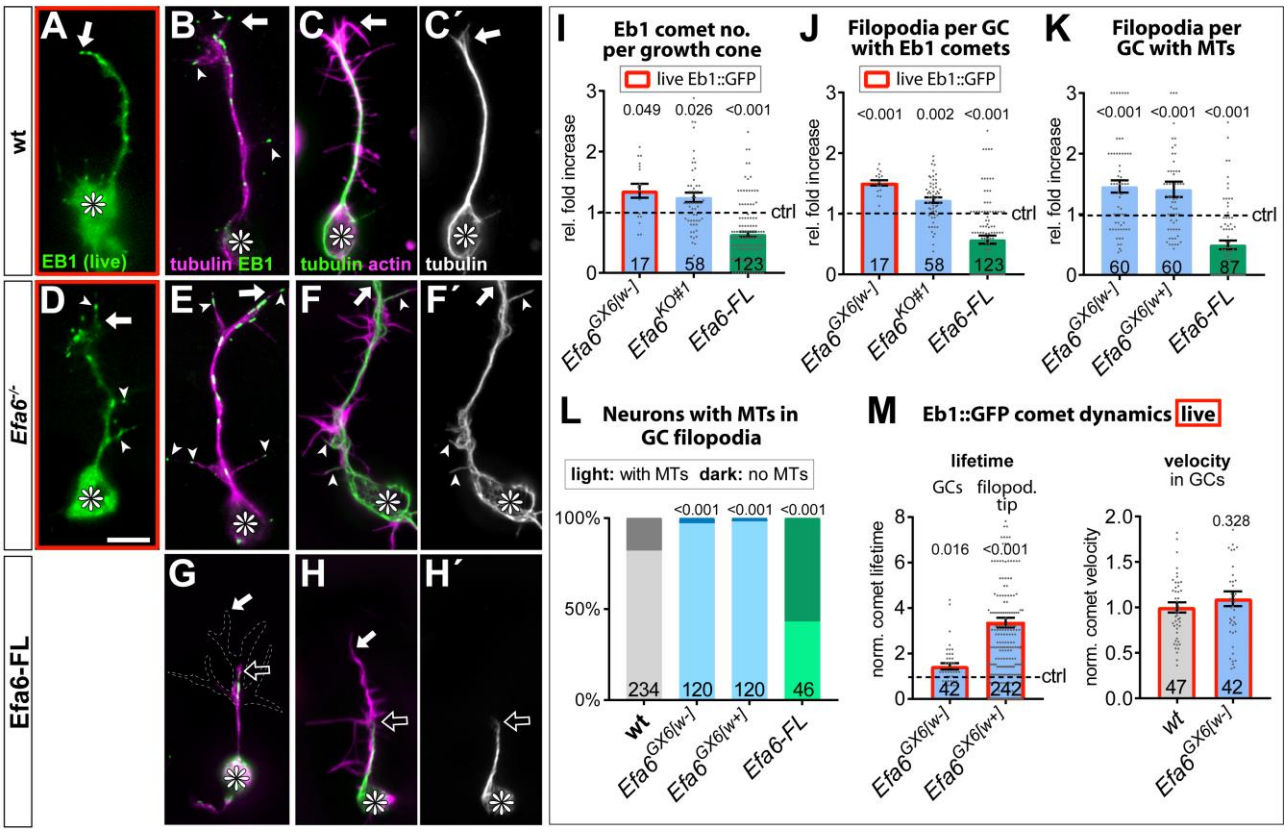

Fig. 4. Efa6 regulates MT behaviours in GCs. **A-H')** Examples of primary neurons at 6HIV which are either wild-type controls (top), Efa6-deficient (middle) or expressing Efa6-FL::GFP (bottom); neurons were either imaged live for Eb1::GFP (green in A,D) or fixed and labelled for Eb1 and tubulin (B,E,G; as colour-coded) or actin and tubulin (C,F,H; as colour coded; tubulin shown as single channel image on the right); asterisks indicate cell bodies, white arrows the tips of GCs, open arrows the tips of MT bundles and arrow heads MTs or Eb1 comets in filopodial processes; the GC in G is outlined with a white dashed line; scale bar in D represents 5µm in all images. **I-M)** Quantitative analyses of MT behaviours in GCs of such neurons as indicated above each graph. Different genotypes are colour-coded: grey, wild-type controls; blue, different *Efa6* loss-of-function conditions; green, neurons over-expressing Efa-FL. The graph in L shows percentages of neurons without any MTs in shaft filopodia (dark shade) versus neurons with MTs in at least one filopodium (light shade; P values above bars assessed via Chi^2 tests), whereas all other graphs show single data points and a bar indicating mean ± SEM, all representing fold-increase relative to wild-type controls (indicated as horizontal dashed "ctrl" line; P values above columns from Mann-Whitney tests. Throughout the figure, sample numbers are shown at the bottom of each bar and data obtained from live analyses with Eb1::GFP are framed in red. For raw data see T4, which can be downloaded here: www.prokop.co.uk/Qu+al/RawData.zip.

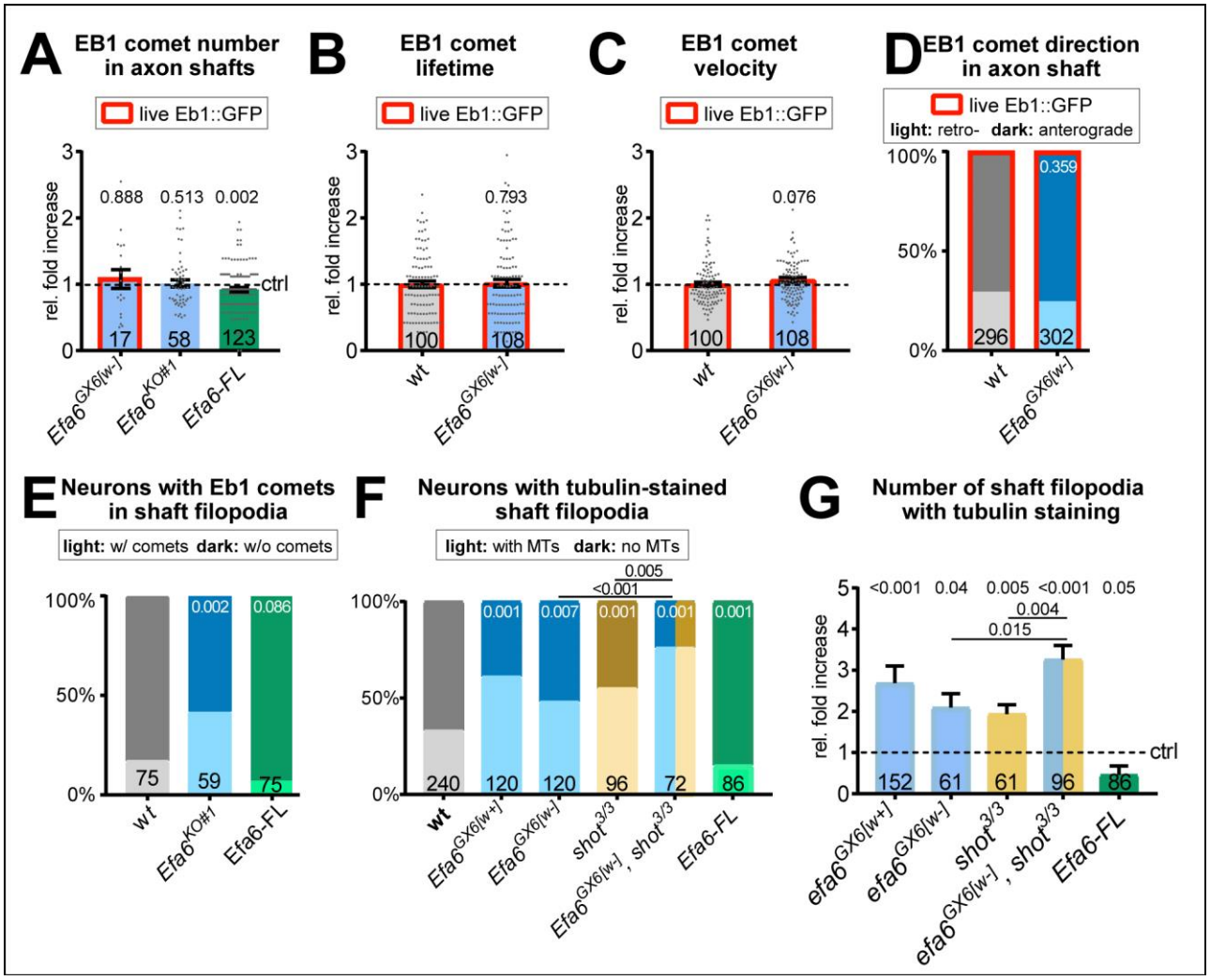

Fig. 5. Loss of Efa6 promotes MT entry into axon shaft filopodia. Quantitative analyses of MT behaviours in axon shafts, as indicated above each graph; bars are colour-coded: grey, controls; blue, different *Efa6* mutant alleles; green, neurons over-expressing Efa-FL::GFP or Efa6::CAAX::GFP; orange, *shot* mutant allele; red outlines indicate live imaging data, all others were obtained from fixed specimens; numbers at the bottom of bars indicate sample numbers, above bars P values. **A-C,G)** Fold-changes relative to wild-type controls (indicated as horizontal dashed "ctrl" line) shown as single data points and a bar indicating mean ± SEM; P values were obtained via Mann-Whitney tests. **D-F)** Binary parameters (light *versus* dark shades as indicated) provided as percentages; P values were obtained via Chi^2 tests. For raw data see T5, which can be downloaded here: www.prokop.co.uk/Qu+al/RawData.zip.

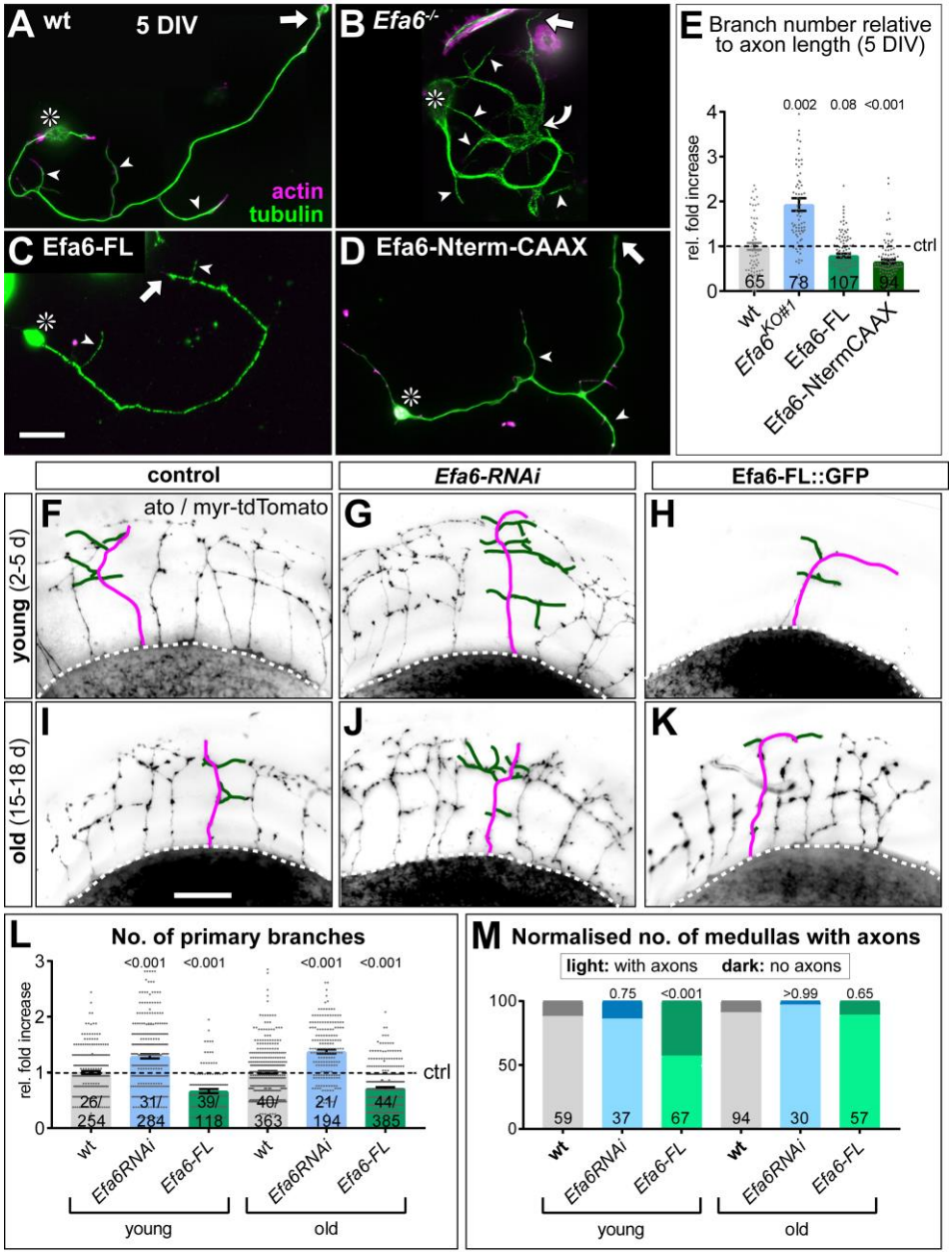

Fig. 6. Efa6 regulates axon branching in in primary *Drosophila* neurons and adult fly brains. Examples of primary *Drosophila* neurons at 5DIV (A-D), all stained for actin (magenta) and tubulin (green); neurons are either wild-type controls (A), Efa6-deficient (B), expressing Efa6-FL::GFP (C), or expressing Efa6-Nterm-CAAX::GFP (D); asterisks indicate cell bodies, arrows point at axon tips, arrow heads at axon branches, the curved arrow at an area of MT disorganisation; the scale bar in C represents 20µm. Quantification of axonal branch numbers (E); different genotypes are colour-coded: grey, wild-type controls; blue, different *Efa6* loss-of-function conditions; green, neurons over-expressing Efa6 variants; data represent fold-change relative to wild-type controls (indicated as horizontal dashed "ctrl" line); they are shown as single data points and a bar indicating mean ± SEM data; P values from Mann-Whitney tests are given above each column, sample numbers at the bottom of each bar. F-K) Brains (medulla region of the optic lobe in oblique view) of young (2-5 d after eclosure; top) and old flies (15-18 d; bottom) driving *UAS-myr-tdTomato* via the *ato-Gal4* driver in dorsal cluster neurons (example neurons are traced in magenta for axons and green for side branches); flies are either wild-type controls (left) or display *ato-Gal4*-driven knock-down of Efa6 (middle) or over-expression of Efa6-FL::GFP (right). L,M) Quantification of data for wild-type (wt; grey), Efa6 knock-down (blue) and Efa6-FL::GFP over-expression (green): L) shows the number of primary branches per axon as fold-change relative to wild-type controls (indicated as horizontal dashed "ctrl" line; data are shown as bars indicating mean ± SEM accompanied by single data points, all normalised to wt); M) displays the number of medullas with axons (light colours) or without axons (dark colours) shown as a percentages in young and old flies. In all graphs, sample numbers at the bottom (in L number of medullas before and number of axons after slash) and P values from Mann-Whitney (G) or Chi^2 tests (H) above each column. Scale bar in D represents 60µm in all figures. For raw data see T6, which can be downloaded here: www.prokop.co.uk/Qu+al/RawData.zip.

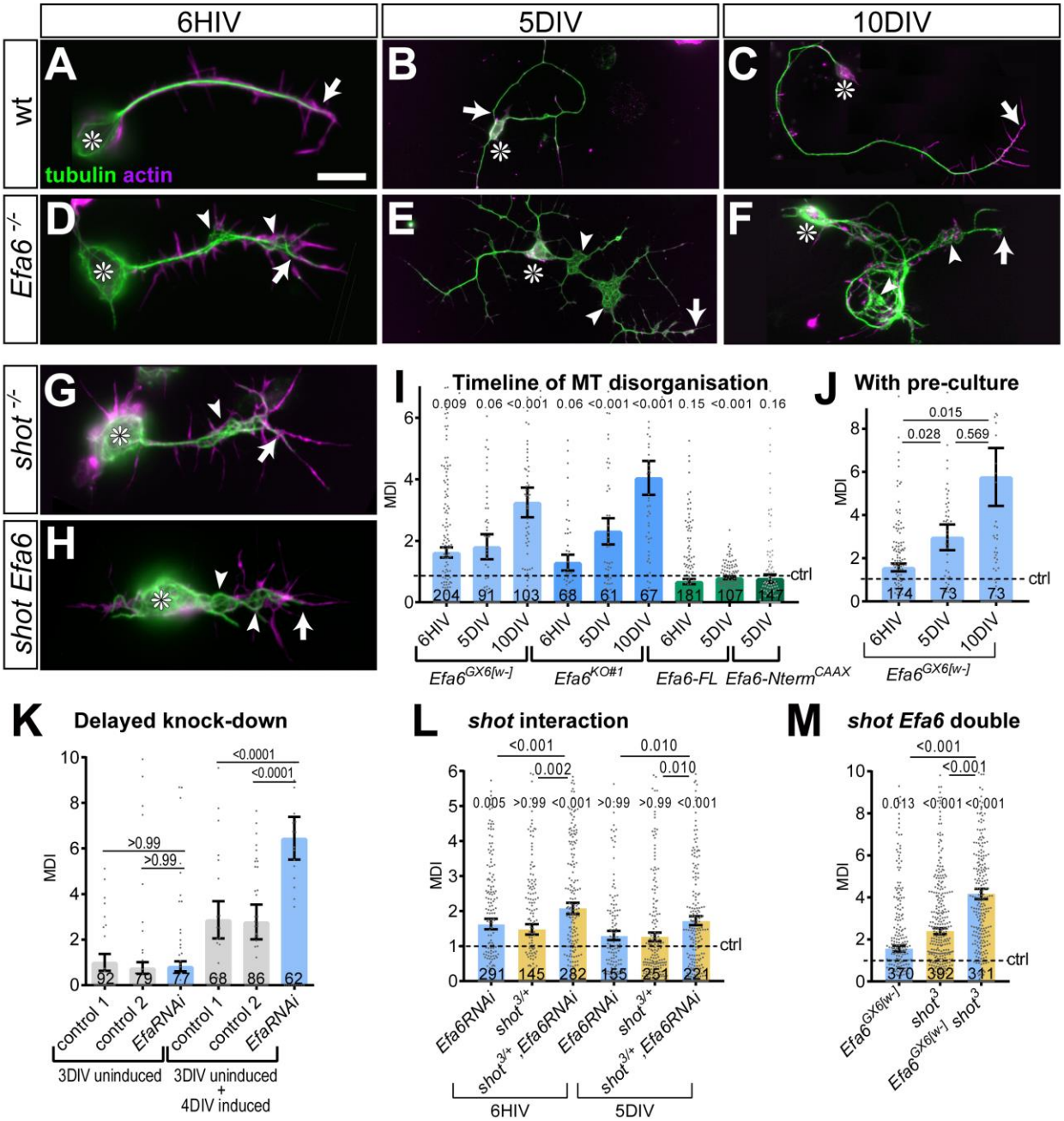

Fig. 7. Efa6 helps to maintain axonal MT bundles in *Drosophila* neurons. **A-H)** Images of primary neurons at 6HIV (left), 5DIV (middle) and 10DIV (right), stained for tubulin (green) and actin (magenta), derived from embryos that were either wild-type (wt, A-C), *Efa6* null mutant (D-F), homozygous for *shot*^{3} (G) or *shot*^{3} *Efa6*$^{GX6[w-]}$ double-mutant (shot Efa6, H); arrows point at axon tip, arrow heads at areas of MT disorganisation, and asterisks indicate the cell bodies; the scale bar in A represents 10µm for 6HIV neurons and 25µm for 5DIV and 10DIV neurons. **I-M)** Quantitative analyses of MT disorganisation (measured as MT disorganisation index, MDI) in different experimental contexts (as indicated above graphs); different genotypes are colour-coded: grey, wild-type controls; blue, *Efa6* loss-of-function; light/dark orange, *shot*^{3} in hetero-/homozygosis; green, neurons over-expressing Efa-FL::GFP or Efa6-NtermCAAX::GFP; data are shown as single data points and a bar indicating mean ± SEM, all representing fold-change relative to wild-type controls (indicated as horizontal dashed "ctrl" line); P values from Mann-Whitney tests in I, J) and Kruskal–Wallis one-way ANOVA with *post hoc* Dunn's test in K-M) are given above each column, sample numbers at the bottom of each bar. Control 1 in (K) is *tub-Gal80*, *elav-Gal4* alone and control 2 *UAS-Efa6RNAi*. For raw data see T7, which can be downloaded here: www.prokop.co.uk/Qu+al/RawData.zip.

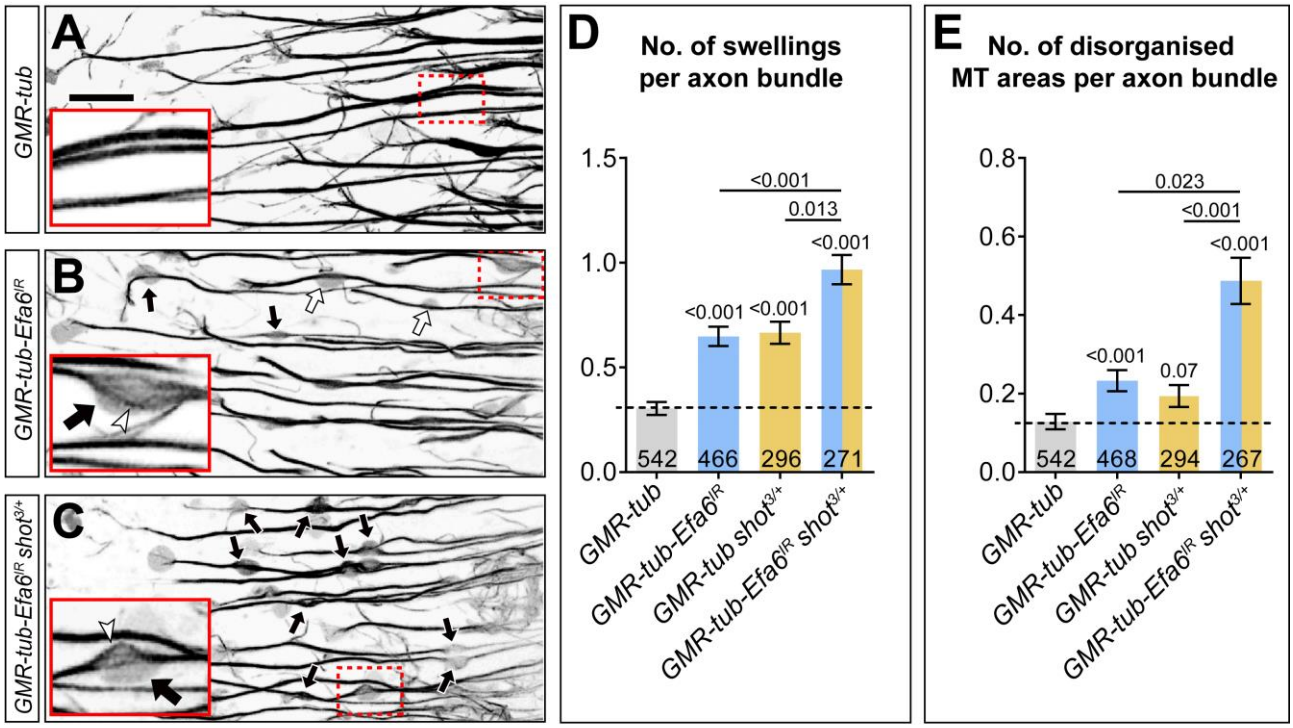

Fig. 8 Efa6 is required for axonal MT bundle maintenance in adult fly brains. A-C) Medulla region of adult brains at 26-27 days after eclosure, all carrying the *GMR31F10-Gal4* driver and *UAS-α-tubulin84B-GFP* (*GMR-tub*) which together stain MTs in a subset of lamina neuron axons that terminate in the medulla. The other specimens co-express *Efa6-RNAi* either alone (*GMR-tub-Efa6^{IR}* in B) or combined with a *shot$^{3/+}$* heterozygous mutant background (*GMR-tub-Efa6^{IR} shot$^{3/+}$* in C). White/black arrows indicate axonal swellings without/with MT disorganisation; rectangles outlined by red dashed lines are shown as 2.5 fold magnified insets where white arrow heads point at disorganised MTs; the scale bar in A represents 15µm in all images. D, E) Quantitative analyses of all axonal swelling (D) or swellings with MT disorganisation (E); different genotypes are colour-coded as indicated; bars show mean ± SEM, all representing fold-change relative to wild-type controls (indicated as horizontal dashed line); P values from Kruskal–Wallis one-way tests are given above each column, sample numbers at the bottom of each bar. For raw data see table T8, which can be downloaded here: www.prokop.co.uk/Qu+al/RawData.zip.

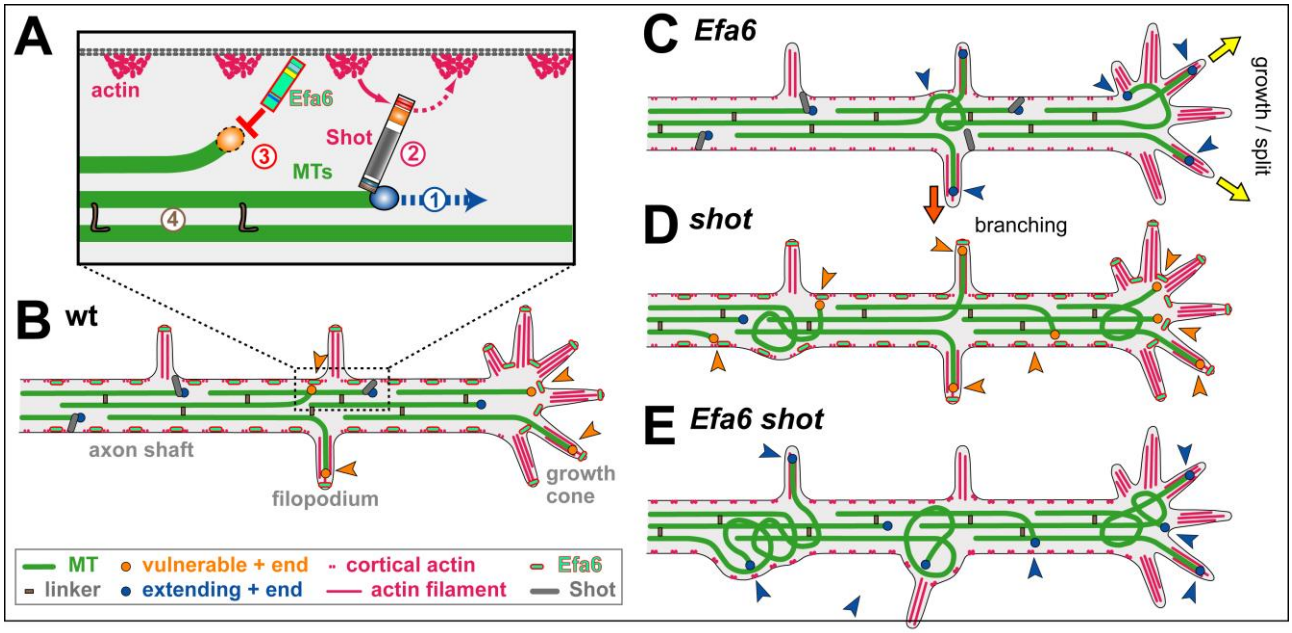

Fig. 9. A model of the suggested roles of Efa6. **A**) The model of local axon homeostasis (Prokop, 2016; Voelzmann et al., 2016a) states that axonal MTs (green bars) are actively kept in bundles; for example, their continued polymerisation (1) mediated by plus end machinery (blue circle) is guided by spectraplakins (here Shot) along cortical actin into parallel bundles (2), or MTs are kept together through cross-linkage (brown "L"; 4; Bettencourt da Cruz et al., 2005; Krieg et al., 2017); here we propose that MTs accidentally leaving the bundle become vulnerable (orange circles) through elimination (red "T") by cortically anchored Efa6. **B**) In normal neurons, polymerising MTs in bundles (dark blue circles) are protected by Shot (marine lines) and MT-MT cross-linkers (brown rectangles), whereas MTs approaches the membrane (orange arrow heads) either by splaying out in GCs or leaving the bundle in the shaft (orange arrow heads) become vulnerable (orange circles) to elimination by Efa6 (light green/red dashes) both along the cortex and in filopodia **C**) Upon Efa6 deficiency, MTs leaving bundles or entering GCs are no longer subjected to Efa6-mediated cortical elimination (blue arrow heads) and can cause gradual build-up of MT disorganisation; when entering shaft filopodia they can promote interstitial branch formation (red arrow), when entering GC filopodia they can promote axon growth or even branching through GC splitting (yellow arrows). **D**) Far more MTs leave the bundles in *shot* mutant neurons, but a good fraction of them is eliminated by Efa6 (increased number of orange arrow heads). **E**) In the absence of both Shot and Efa6, more MTs leave the bundles, but there is no compensating cortical elimination (increased number of blue arrow heads), so that the MT disorganisation phenotype worsens**.**

Supplementary materials

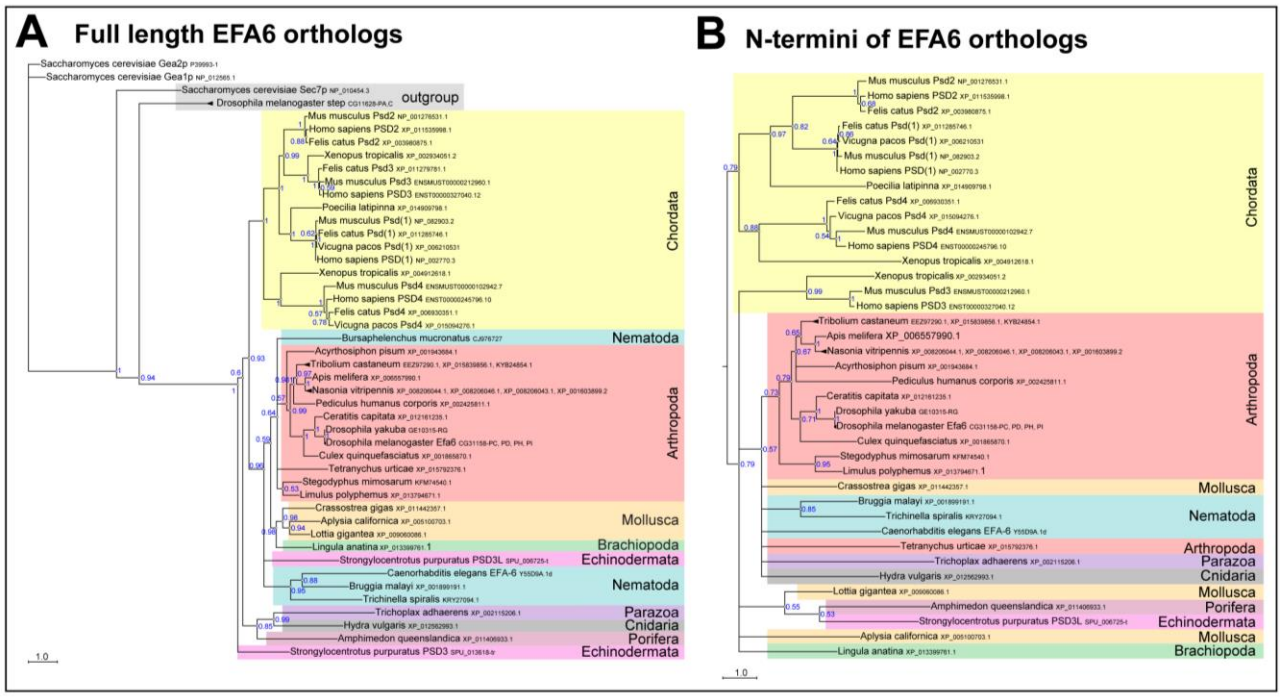

Fig. S1 Phylogentic tree analysis of Efa6. Bayesian phylogenetic analysis of full length (**A**) or N-termini (**B**) of Efa6 orthologues. Sequences were aligned using Muscle or ClustalO and posterior probabilities and branch lengths calculated using MrBayes. Branch length scale is indicated; blue numbers show posterior probabilities of each branch split. For the full length tree, *Drosophila steppke* (*step*) was used as outgroup (Hahn et al., 2013). In both full length and N-terminus analyses, chordates (cream colour) split off very early from Efa6 versions of other species, in line with an early speciation event separating both groups before the vertebrate multiplication events took place. Phyla are highlighted in different colours, gene symbols and/or accession numbers are given after the species names.

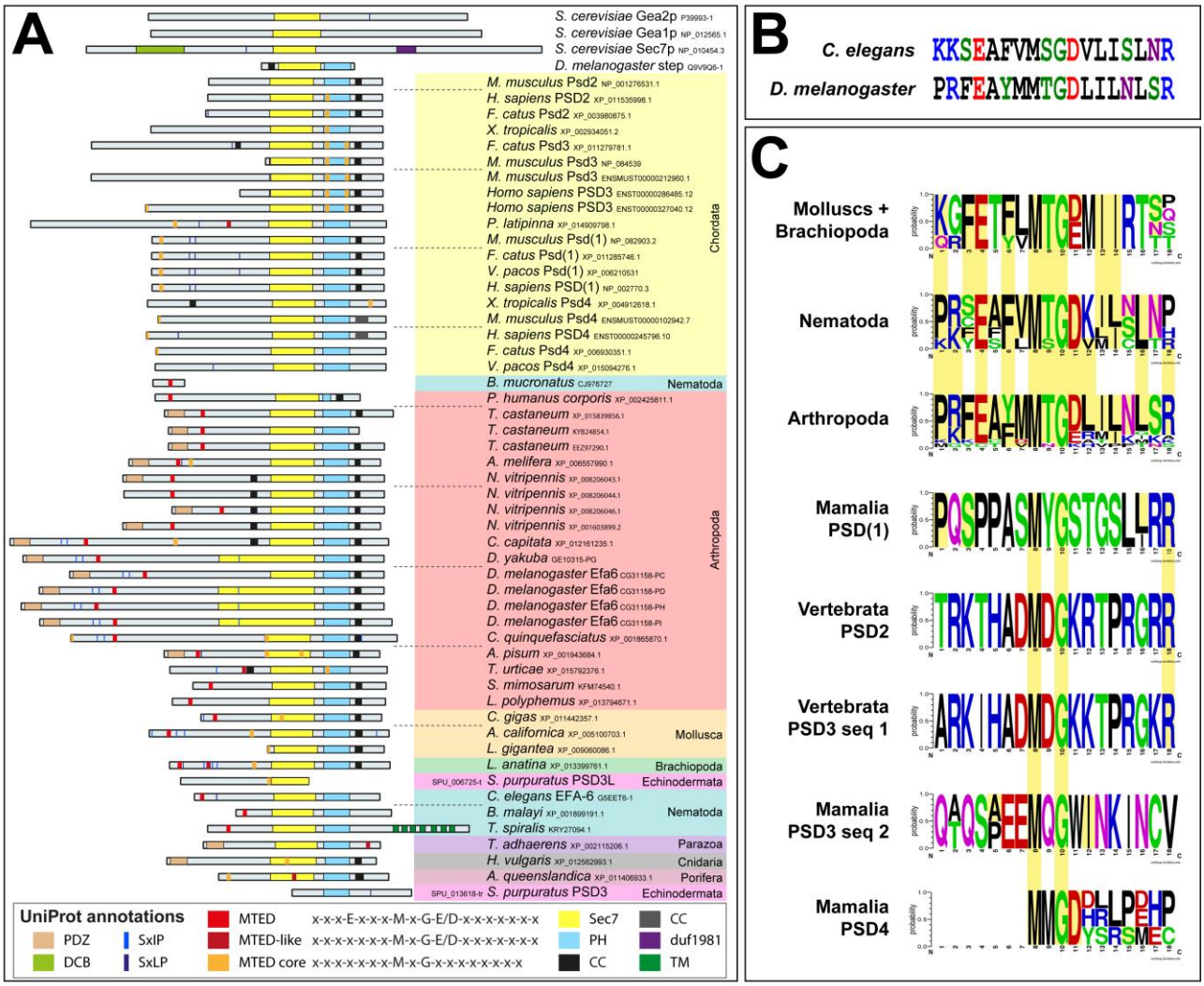

Fig. S2. Efa6 N-terminal domains vary amongst different phyla. **A)** Domain annotations in 56 Efa6 orthologues via EMBL SMART and Uniprot. Phyla are colour-coded as in Fig.S1. Note that there is a strong variation of lengths and domain composition in particular of the N-terminus. The putative PDZ domain seems to be a feature mainly of insect versions of Efa6 and is absent from any analysed chordate orthologues; MTED and MTED-like sequences cannot be consistently identified in all Efa6 orthologues and are very divergent in chordate Efa6/PSD versions. SxIP/SxLP sites [flanked by positive charges as would be expected of functional motifs (Honnappa et al., 2009)] are found in the N-terminal half of only a subset of Efa6 versions in nematodes (e.g. *C. elegans*), insects (in particular flies, e.g. *D. melanogaster*) and molluscs, and even fewer in chordates; in mouse, alpaca and cat SxIP/SxLP sites are flanked by negative charges. **B)** To determine a potential MTED consensus sequence, 37 sequences of molluscs, nematodes, arthropods and putative MTED sequences of mammalian PSD1-4 were grouped according to phylum; consensus sequences were depicted using Berkley's Weblogo online server (default colour scheme). Amino acid positions identical to *D. melanogaster* and *C. elegans* MTED are highlighted (faint yellow).

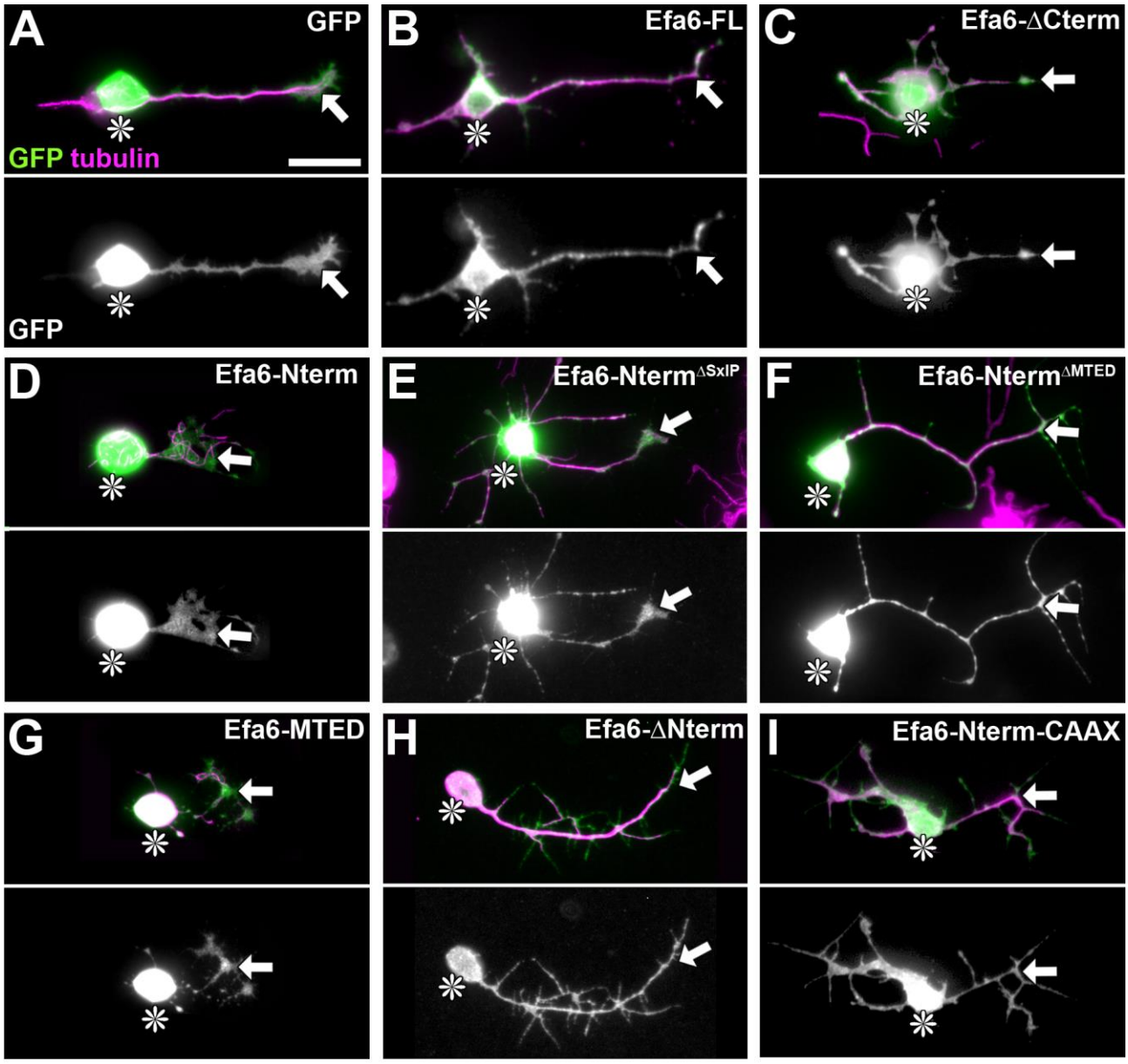

Fig.S3. Localisation of Efa6 constructs in primary neurons. Images show transfected primary *Drosophila* neurons at 18HIV stained for tubulin (magenta) and GFP (green and in greyscale below the colour image). Cell bodies are indicated by asterisks, axon tips by arrows. The transfected constructs are indicated top right following the nomenclature explained in Fig.3B. Scale bar in A represents 10µm for all figures shown.

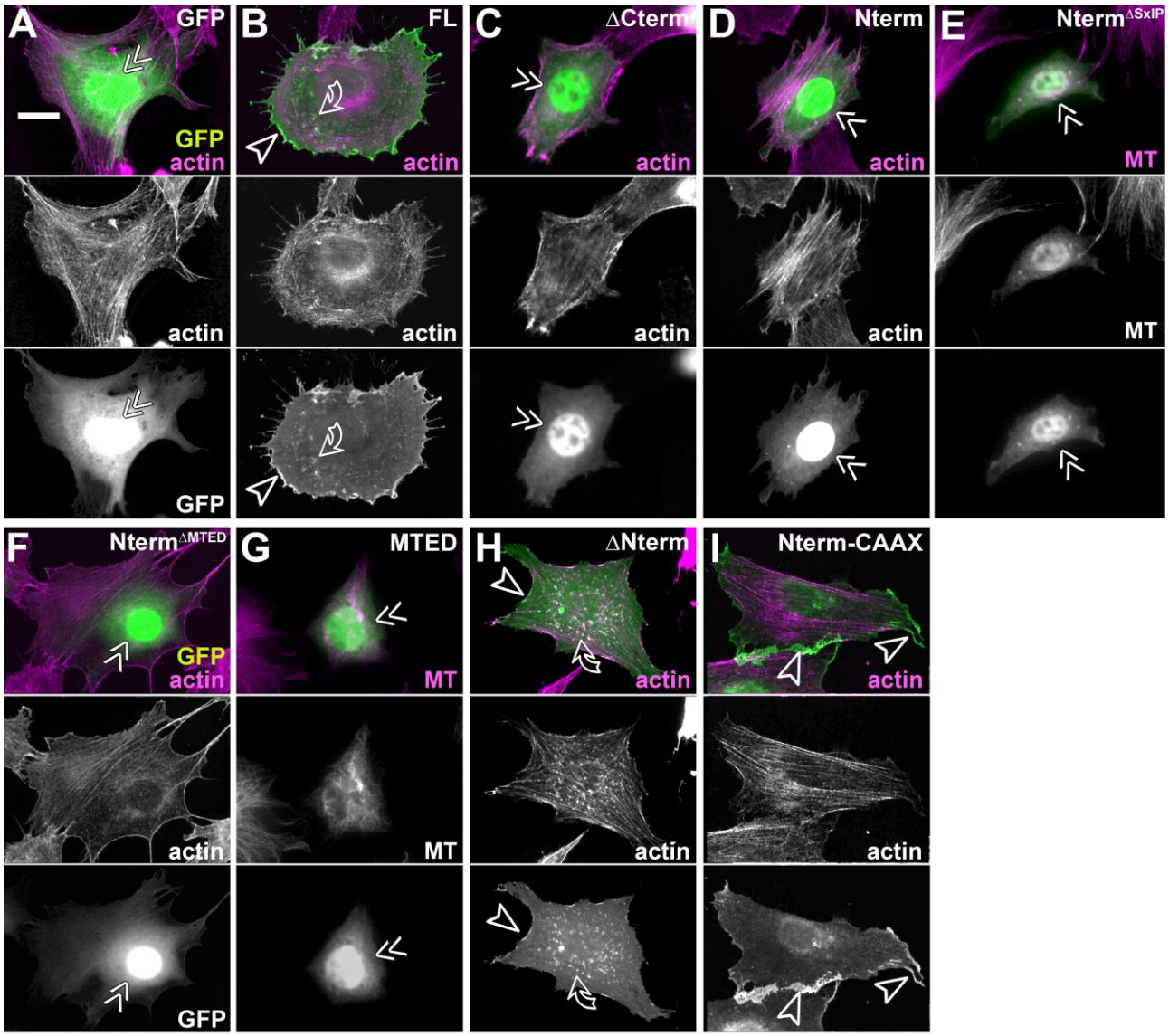

Fig.S4. Efa6 constructs localisations in fibroblasts. Images show fibroblasts which are all stained for GFP (green) and either for actin or MTs (magenta); GFP and actin/MTs shown as single channels in greyscale below the colour image, 24hrs after transfection with control (GFP) or Efa6-derived constructs (nomenclature as explained in Fig.3B, but leaving out the “Efa6“-prefix and “::GFP”-postfix, as indicated top right. Double chevrons indicate nuclear localisation, arrow heads membrane localisation apparent at cell edges and curved arrows membrane ruffles. Scale bar in A represents 10µm in all images.

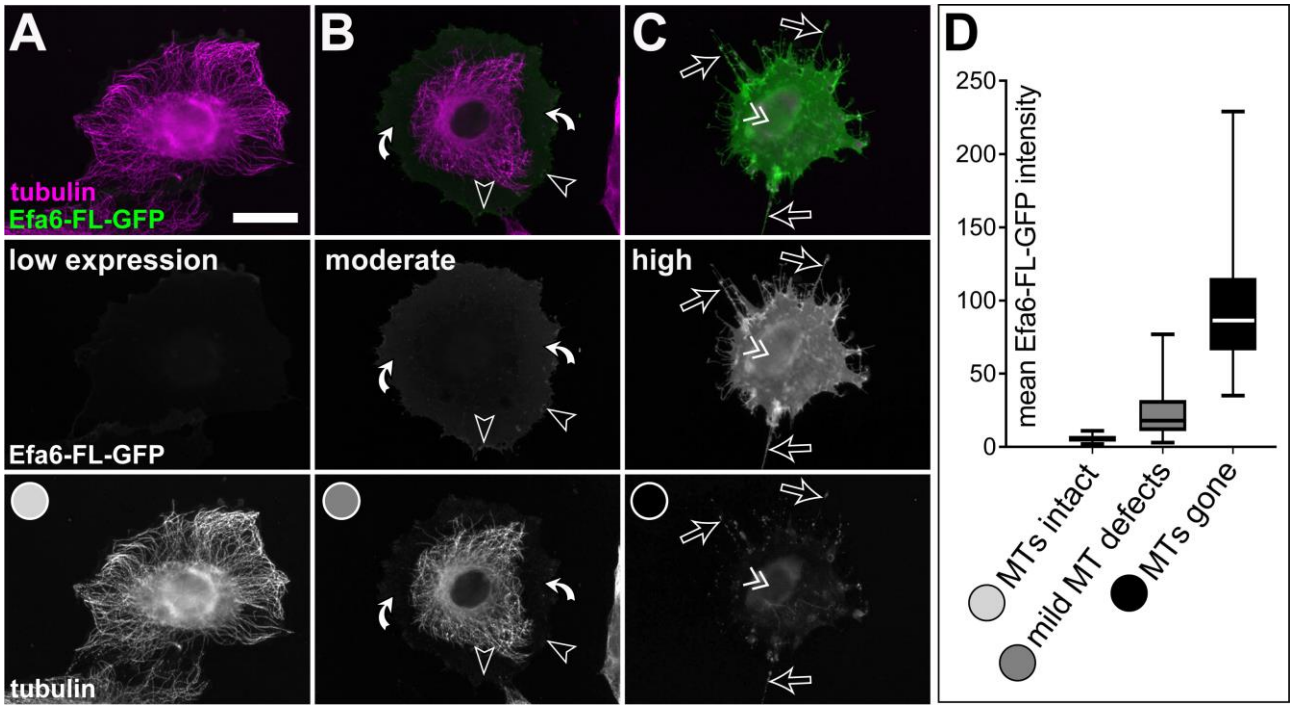

Fig.S5. MT elimination by Efa6-FL is concentration-dependent in fibroblasts. **A-C)** Representative images of fibroblasts stained for GFP and tubulin (green and magenta, respectively; both shown as single channels in greyscale below the colour image). Images were taken 24hrs after transfection with *Efa6-FL::GFP*, assessed for GFP intensity (plotted on the ordinate in **D**; examples for low, moderate and high expression are given in the left, middle and right columns, respectively) and then grouped with respect to their MT phenotypes into "MTs intact" (light grey), "mild MT defects" (medium grey) or "MTs gone" (black), as indicated by greyscale circles in the lowest row of A-C and the abscissa of D. Arrow heads point at GFP accumulation at membrane edges, white curved arrows indicate areas of the cell from where MTs have retracted, open arrows point at retraction fibres and the double chevron indicates the nucleus position and signs of nuclear GFP localisation. Scale bar in A represents 10µm in all images. For raw data see T9, which can be downloaded here: www.prokop.co.uk/Qu+al/RawData.zip.

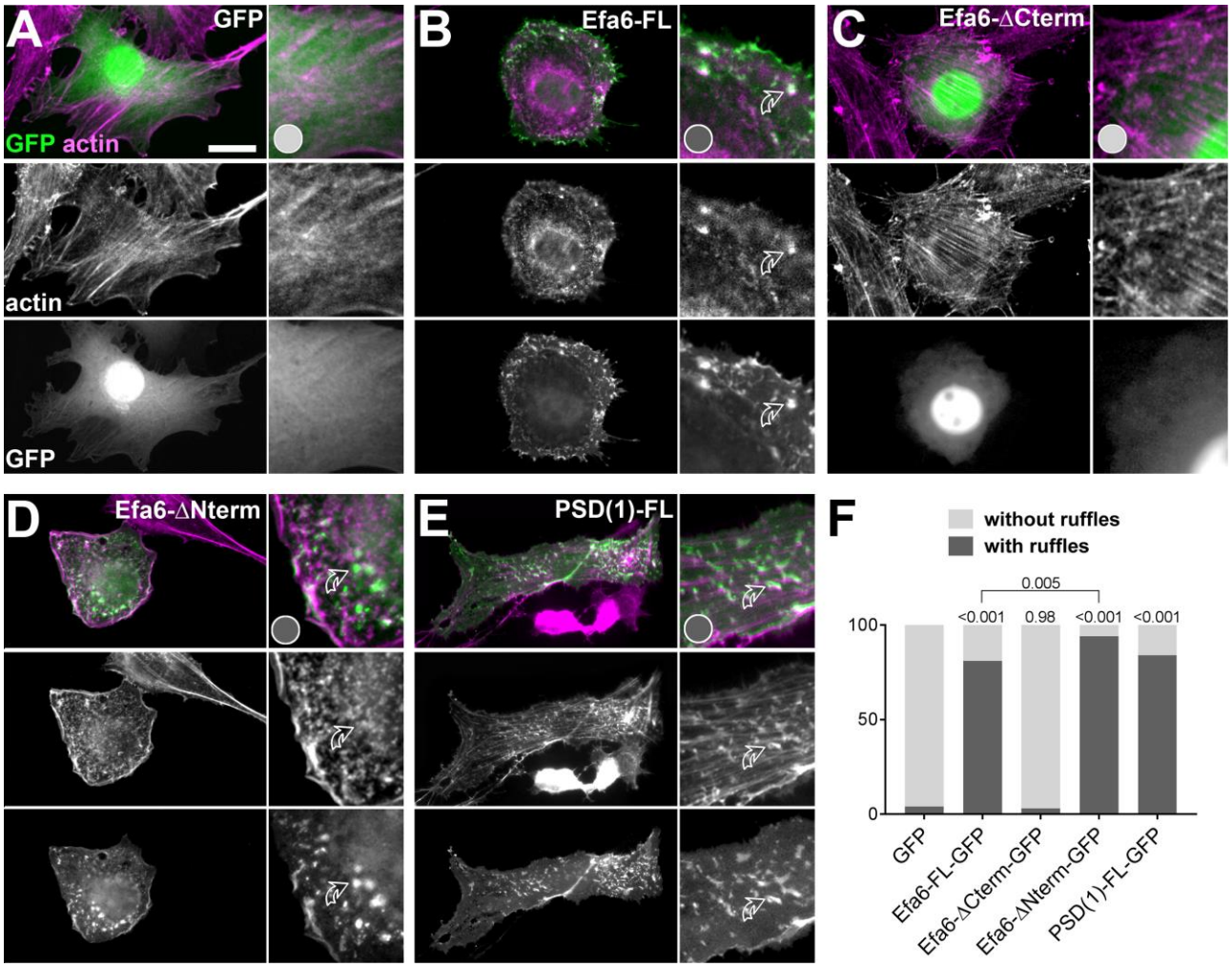

Fig. S6. Conserved functions of the Efa6 C-terminus in membrane ruffle formation. **A-E)** Representative images of fibroblasts stained for GFP and actin (green and magenta, respectively; both shown as single channels in greyscale below the colour image). Images were taken 24hrs after transfection with different constructs (indicated top right): control vector (GFP; A), Efa6-derived constructs (B-D; nomenclature as explained in Fig.3B, but leaving out the "Efa6"-prefix and "::GFP"-postfix) or PSD1-FL::GFP (E). To the right of each image, a selected area is displayed with 2.5-fold magnification, showing dotted actin- and GFP-stained ruffles (curved open arrows) in B, D and E, but not A and C; ruffle formation has been quantified and is shown as a bar graph in **F**. All graph bars indicate percentages of fibroblasts with/without membrane ruffles (dark/light grey); P values on top of bars are from Chi^2 tests relative to GFP controls. As shown, ruffle phenotype were never observed with any N-terminal Efa6 variants but are reproduced with the Efa6-ΔNterm::GFP variant (comprising the C-terminal Sec7, PH and CC domains; Fig. 3B). Scale bar in the top image of A represents 10 µM for all fibroblasts shown. For raw data see T10, which can be downloaded here: www.prokop.co.uk/Qu+al/RawData.zip.

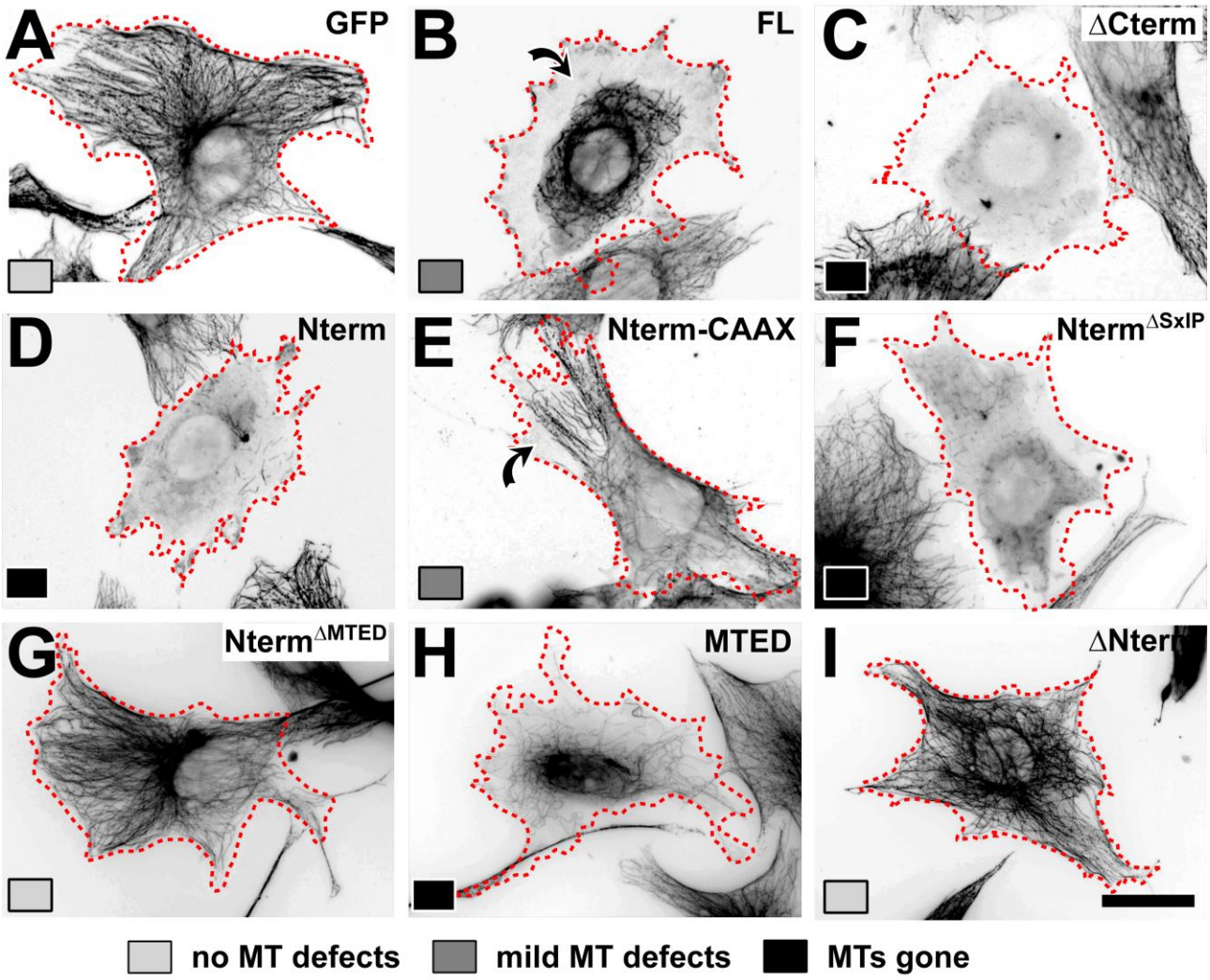

Fig. S7. Representative MT phenotypes induced by the different constructs in transfected fibroblasts. Fibroblasts 24hrs after transfection with different control (GFP) or Efa6-derived constructs as indicated top right in each image (nomenclature as explained in Fig.3B, but leaving out the "Efa6"-prefix and "::GFP"-postfix). Cells were stained for tubulin (black; images shown as inverted greyscale) and classified as "no MT defects" (light grey), "mild MT defects" (medium grey) or "MTs gone" (black), as indicated by greyscale boxes bottom left of each image; curved arrows indicate peripheral MT depletion. Each image represents the most prominent phenotype for each respective construct. Scale bar at the bottom right in H represents 25µm in all images.

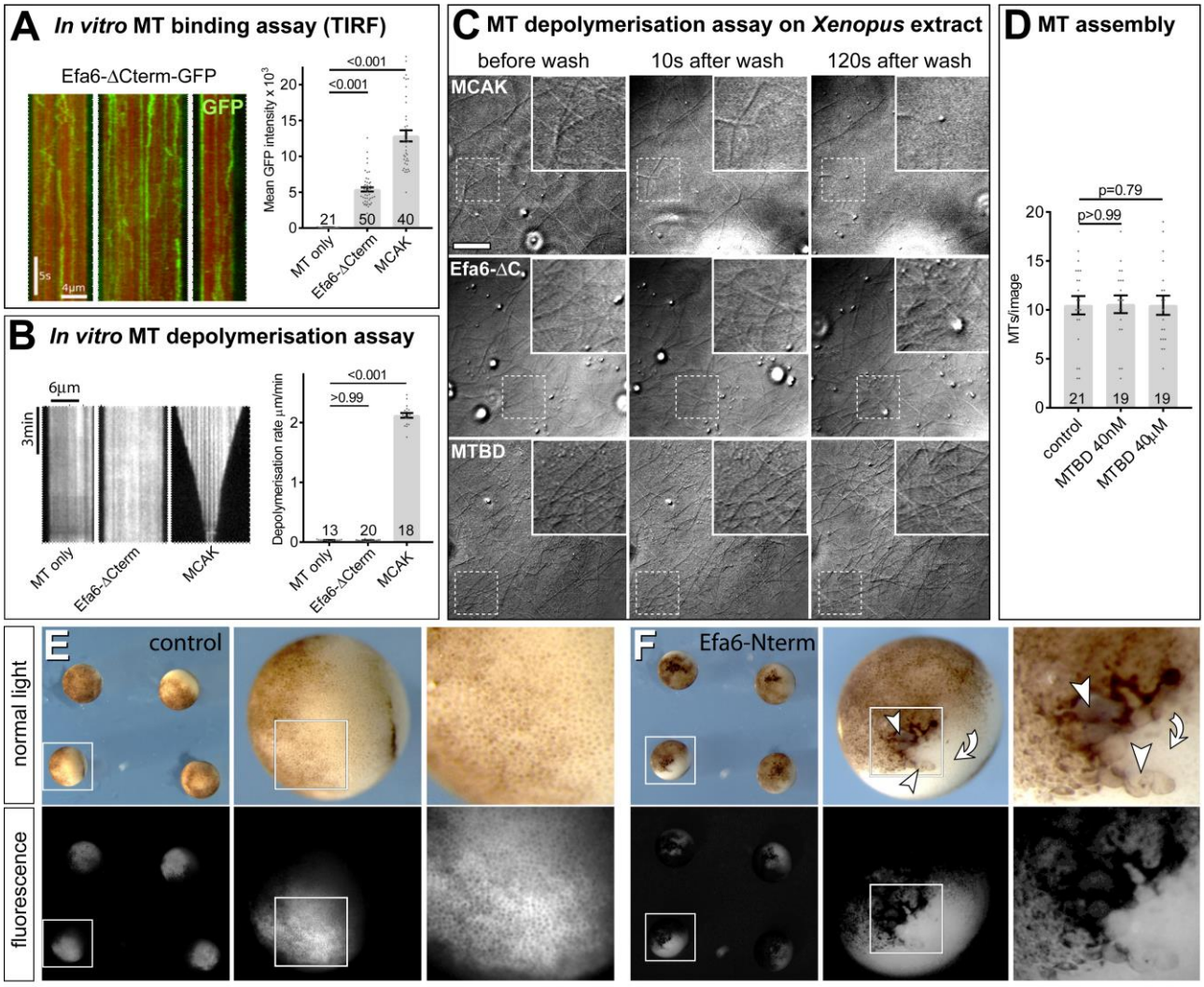

Fig. S8. *In vitro* attempts to resolve the MT elimination mechanism of Efa6. **A)** To determine whether Efa6 directly affects MT stability, we recombinantly expressed Efa6-ΔCterm::GFP in Sf9 cells, purified the protein and observed its interaction with MTs using total internal reflection fluorescence (TIRF) microscopy in a low ionic strength buffer (BRB20, 75mM KCl); images on the left show three examples of kymographs of MT lattices decorated with Efa6-ΔCterm::GFP, which displays a mixture of stationary molecules and diffusive interactions typical of non-translocating MT-associated proteins (Helenius et al., 2006; Hinrichs et al., 2012); bar charts (right) show quantification of the amount of interacting protein: background signal from MTs alone, Efa6-ΔCterm::GFP (20nM) and the non-translocating kinesin MCAK::GFP (20nM) as positive control; at the same protein concentration, over 2-fold more molecules of MKAC typically interact with MTs; all graphs in this figure show individual data points and bars representing mean ± SEM; numbers above bars show P values obtained from Mann–Whitney Rank Sum statistical analyses, numbers in bars the respective sample numbers. **B)** Kymographs (left) show individual fluorescently-labelled GMPCPP-stabilised MTs *in vitro* (Patel et al., 2016), either alone (MTs only; basal depolymerisation rate, n=7) or in the presence of 14 nM Efa6-ΔCterm::GFP (n=8) or 40nM MCAK::GFP (n=18); the bar chart (right) quantifies the induced depolymerisation rates; using two different purifications of Efa6-ΔCterm::GFP on three separate occasions, we saw no evidence of MT depolymerisation above the basal level of depolymerisation typically observed in these assays, whereas parallel control experiments with mitotic centromere-associated kinesin/MCAK showed MT depolymerisation rates typical of this kinesin. **C)** To assess whether MT destabilisation might require additional cytoplasmic factors, we used *Xenopus* oocyte extracts: phase contrast images show MTs in *Xenopus* oocyte extracts (after they had been allowed to polymerise for 20 min) and then showing stills from before, 10s after and 120s after washing in 20nM MCAK::GFP (as positive control), 20nM Efa6-ΔCterm::GFP or 40nM synthetic MTED (to overcome potential mis-folding of the purified ΔCterm protein); squares outlined by dashed white lines are shown magnified in insets revealing MTs; MTs clearly vanish upon treatment with MCAK, but counts of MTs did not reveal any obvious effects on MTs with either of the Efa6 peptides. **D)** Finally, interference with MT polymerisation was analysed by adding 20nM MTED to diluted *Xenopus* cytosol, and 20 random fields were recorded 10 min later via VE-DIC microscopy and the numbers of MTs per field counted; data plots show that MTED does not interfere with MT polymerisation. **E, F)** *RFP* controls and *Efa6-Nterm::GFP* expression

constructs were injected into *Xenopus* embryos at the 4-cell stage and analysed 24 hrs later; only the *Efa6* construct caused a strong suppression of cell division, as indicated by the presence of very large cells (arrows) and pigmentation defects (curved arrows) at the site of injection, suggesting that Efa6-Nterm::GFP is functional when expressed in the *Xenopus* context. Taken together, the very different data obtained in *Xenopus* cytosol *in vitro* or embryos *in vivo*, suggest that either the effect of Efa6 requires a factor absent from Xenopus extract or that Efa6-ΔCterm::GFP and MTED are non-functional due to mis-folding. The latter is suggested by the observation of many aggregates of Efa6-ΔCterm::GFP in A. Scale bar (in top left image) represents 3 µm in C (2.5 fold magnified insets), and 1400 µm / 350 µm / 140 µm in left / middle / right images of E and F, respectively. For raw data see T11, which can be downloaded here: www.prokop.co.uk/Qu+al/RawData.zip.

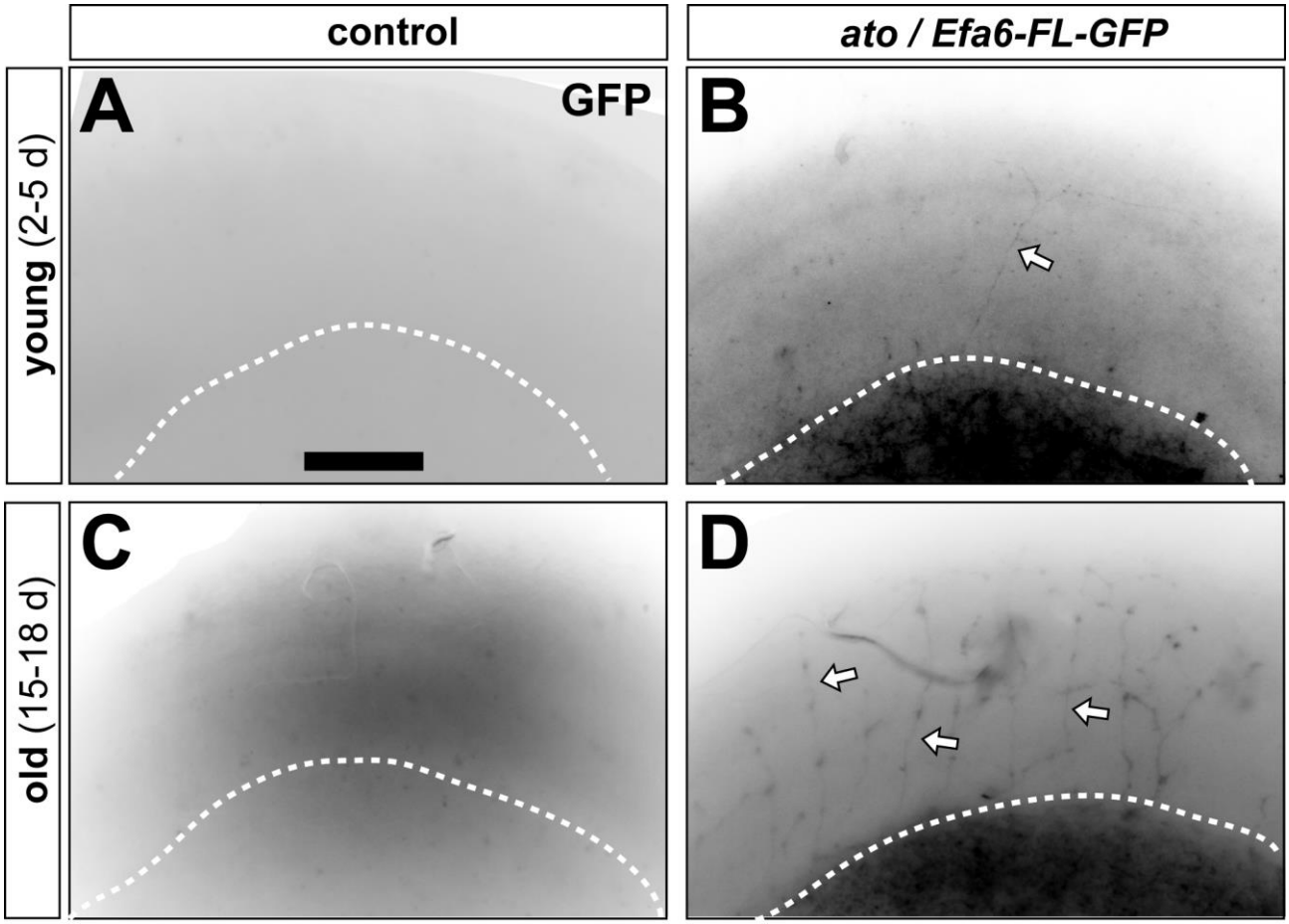

Fig.S9 *ato-Gal4*-driven Efa-FL::GFP expression in adult brains. Brains (region of the optic lobe in oblique view; white dashed line indicating the lower edge of the medulla) of young (2-5 d after eclosure; top) and old flies (15-18 d; bottom) which are either from wild-type controls or from flies driving *UAS-myr-tdTomato* and *UAS-Efa6-FL-GFP* via the *ato-Gal4* driver in dorsal cluster neurons; specimens are stained for GFP and arrows point at stained; for myr-dtTomato staining of brains from these experiments see Fig.6F-K. Scale bar in D represents 60µm in all images.

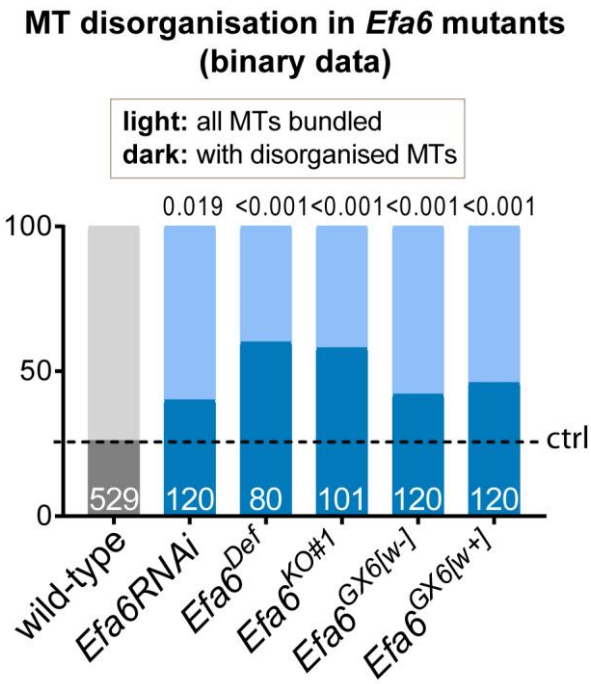

Fig. S10. Efa6 mutant primary neurons show MT disorganisation. Quantitative analyses of MT disorganisation measured as binary score: percentages of neurons with bundled MTs throughout (light colour) or showing obvious MT disorganisation in their axons (dark colour) in different *Efa6* mutant alleles (control value indicated as horizontal dashed "ctrl" line); P values from Chi^2 tests are given above the bars. For raw data see T12, which can be downloaded here: www.prokop.co.uk/Qu+al/RawData.zip.

Suppl. Movie M1. Eb1::GFP in mouse NHTH3 fibroblast about 6 hours after transfection. Pictures for the movie were taken at 2 s intervals. Scale bar indicates 10 µm. Movie available at http://www.prokop.co.uk/Qu+al/SupplMov.html.

Suppl. Movie M2. Eb1::GFP in a growth cone of a wild-type *Drosophila* primary neuron at 6 HIV. Arrows indicate positions where individual Eb1::GFP comets terminate. Pictures of the movie were taken at 2 s intervals. Scale bar indicates 10 µm. Movie available at http://www.prokop.co.uk/Qu+al/SupplMov.html.

Suppl. Movie M3. Eb1::GFP in a growth cone of a wild-type *Drosophila* primary neuron at 6 HIV. Arrows indicate positions where individual Eb1::GFP comets terminate. Pictures of the movie were taken at 2 s intervals. Scale bar indicates 10 µm. Movie available at http://www.prokop.co.uk/Qu+al/SupplMov.html.

Suppl. Movie M4. Eb1::GFP in a growth cone of an *Efa6* $^{GX6[w-]}$ mutant *Drosophila* primary neuron at 6 HIV. The arrow heads follow individual Eb1::GFP comets illustrating either their trajectories adjacent to the membrane or prolonged dwell time at filopodial tips. Pictures for the movie were taken at 2 s intervals. Scale bar indicates 10 µm. Movie available at http://www.prokop.co.uk/Qu+al/SupplMov.html.

Suppl. Movie M5. Eb1::GFP in a growth cone of an *Efa6* $^{GX6[w-]}$ mutant *Drosophila* primary neuron at 6 HIV. The arrow heads follow individual Eb1::GFP comets illustrating either their trajectories adjacent to the membrane or prolonged dwell time at filopodial tips. Pictures for the movie were taken at 2 s intervals. Scale bar indicates 10 µm. Movie available at http://www.prokop.co.uk/Qu+al/SupplMov.html.